Proliferation and prohibition of self-loops in ensembles of interacting binary elements

Paul Baconnier,[1] Margot H. Teunisse,[1,2] and Martin van Hecke[1,2]

[1] *AMOLF, 1098 XG Amsterdam, The Netherlands.*
[2] *Huygens-Kamerlingh Onnes Laboratory, Leiden University, 2300 RA Leiden, The Netherlands.*

Models based on spins or hysterons with appropriately chosen interactions can capture advanced memory effects in complex materials, such as transients in repeatedly compressed crumpled sheets or sequential computing in driven metamaterials. However, unphysical self-loops dominate the response when interactions are chosen randomly, undermining statistical approaches. Here, we uncover the origin of self-loop proliferation in randomly coupled models. We introduce the weakly asymmetric ensemble to suppress self-loops and then develop interaction ensembles to strictly eliminate these. Finally, we use these ensembles to explore the statistics of large systems. Our work highlights the subtle role of interaction symmetries and paves the way for statistical studies of the sequential response and memory effects in complex, multistable materials.

Sequences of transitions between metastable states govern the hysteresis [1], memory [2–9], emergent computing [10–12], sequential shape-morphing [13, 14], and adaptive behavior [15–17] of driven dissipative materials, such as crumpled sheets, disordered media, and metamaterials [9]. As these states often consist of local, binary elements, with or without hysteresis, the response can be described by models of interacting hysterons or binary spins at zero-temperature (Fig. 1a). While models without interactions are well understood [1, 18–20], interactions are crucial for capturing complex responses such as avalanches, transients, and multiperiodic cycles [5, 21]. In the rare cases that interactions can be measured [7, 10] or modeled [12, 22–26], they enable accurate predictions of the systems response and memory effects [5, 8, 10, 12, 26–28]. However, often the detailed interactions are unknown. Moreover, an important goal is to understand classes of system through statistical studies of ensembles of interaction coefficients [4, 5, 21, 29–31].

The focus of this Letter are self-loops, avalanches that get trapped in a repeating sequence of states which never settle (Fig. 1b) [21, 32–35]. These overwhelm the response in large randomly coupled systems, yet are unphysical for the dissipative systems we aim to model.

The interaction matrix c_{ij} represents how element i's flipping threshold is influenced by element j, and its symmetry plays an important role. For spin systems, symmetric interactions produce transitions that lower an energy and are thus free of self-loops [34, 36], and we show here a similar result for symmetrically interacting hysterons. For spins, non-symmetric interactions have been associated with energy input and drive oscillations or self-loops [32–35, 37–41]. However, for hysterons, asymmetric interactions are not incompatible with energy dissipation. As hysterons are strongly nonlinear, the Maxwell-Betti reciprocity relations no longer apply [42] and do not restrain c_{ij} to be symmetric. Instead, the asymmetry of the interaction matrix arises from differences in hysteron strength. For example, in a crumpled sheet, flipping a hysteron associated with a small ridge (i) weakly affects a larger ridge (j), while flipping hysteron j more strongly impacts i: $|c_{ij}| < |c_{ji}|$ (Fig. 1c). Indeed, when measured or modeled, hysteron interactions are asymmetric [10, 12, 26], and asymmetry is crucial to capture observed

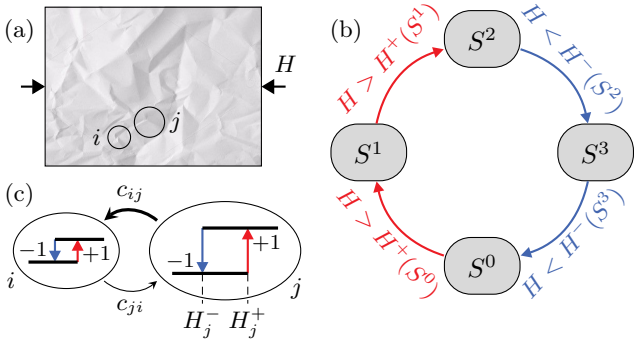

FIG. 1: Self-loops in driven multistable systems. (a) Schematic of a crumpled sheet where local ridges act as hysterons [7]. (b) Partial transition graph. The states $(S^0, S^1, \dots)$ undergo transitions when the driving H crosses the indicated switching fields (up: red, down: blue). If the system starts in state S^0 and H is increased above the switching field $H^+(S^0)$, this causes the self-loop $S^0 \to S^1 \to S^2 \to S^3 \to S^0 \to \dots$ when the switching fields satisfy $H^+(S^1) < H^+(S^0)$, $H^-(S^2) > H^+(S^0)$ and $H^-(S^3) > H^+(S^0)$ (Supplemental Material). (c) Variations in hysteron strength lead to asymmetric interactions ($|c_{ij}| > |c_{ji}|$).

memory effects [5]. We thus face a conundrum: while asymmetry is necessary, random asymmetric interactions lead to self-loops inconsistent with dissipative behavior.

Here we first uncover the mechanisms that produce self-loops and investigate their proliferation. We then explore self-loops for asymmetric interactions and show that their probability asymptotes to one in large systems. We explore strict conditions associated with specific self-loops, derive precise criteria for short self-loops, and introduce weak asymmetry as a simple, lenient approach to suppress self-loops. We then present several strict ensembles that are completely free of self-loops. Finally, we explore the statistical properties of avalanches and the response to cyclic driving in large systems. Our work opens the route towards statistical studies of the sequential response of dissipative materials.

Model.— We consider N binary elements, $s_i = \pm 1$, which form collective states $S = (s_1, s_2, \dots)$. The system is driven by a global field H, and the stability range of each element i in state S is given by switching fields

$H_i^{\pm}(S)$. For pairwise interactions:

$$H_i^{\pm}(S) = h_i^{\pm} - \sum_{j \neq i} c_{ij} s_j \ , \tag{1}$$

where $h_i^{\pm}$ are the bare switching fields of element i. To model spins, we take $h_i^+ = h_i^-$, whereas for hysterons, $h_i^+ > h_i^-$ [1, 19, 20]. The matrix c_{ij}, with $c_{ii} = 0$, encodes cooperative ($c_{ij} > 0$) or frustrated ($c_{ij} < 0$) interactions that may be asymmetric ($c_{ij} \neq c_{ji}$) [5, 12, 26, 28].

In this model, each state S has a range of stability, encoded in state switching fields $H^{\pm}(S)$ which follow from the extrema of $H_i^{\pm}(S)$: $H^+(S) := \min_{i^-}(H_i^+(S))$ and $H^-(S) := \max_{i^+}(H_i^-(S))$, where $i^{\pm}$ are the indices where $s_i = \pm 1$. When the system is in state S^0 and H is increased above $H^+(S^0)$ or decreased below $H^-(S^0)$, state S^0 loses stability and its unstable hysteron flips. Depending on n_u, the number of unstable hysterons in the resulting state S^1, three different scenarios arise [21, 31]. When $n_u = 0$, state S^1 is stable; when $n_u = 1$, state S^1 is unstable and its unstable hysteron flips; when $n_u > 1$, multiple hysterons are unstable. The latter case, which is abundant in large systems (Supplemental Material), leads to a race condition, and requires a dynamical rule to specify the next step in the transition [10, 12, 21, 28, 31]. Importantly, in the remainder, we only flip the most unstable element [5]; this rule is physically plausible and corresponds to the zero-temperature limit of the Glauber dynamics [43, 44] (for other rules, which can have a drastic impact, see Supplemental Material).

Hysterons with symmetric interactions.— Although hysteron interactions are not expected to be symmetric, numerical sampling reveals that symmetric interactions consistently avoid self-loops. To rigorously demonstrate this, one can show that the quantity $V(S)$, written as:

$$\begin{aligned} V(S) = &- \sum_{i^-} \left[s_i (H - h_i^+) + \frac{1}{2} \sum_{j \neq i} c_{ij} s_i s_j \right] \\ &- \sum_{i^+} \left[s_i (H - h_i^-) + \frac{1}{2} \sum_{j \neq i} c_{ij} s_i s_j \right] , \end{aligned} \tag{2}$$

is a Lyapounov function of the system, which guarantees that the latter always converges toward a stable state, and thus prohibits self-loops. (see Appendix A)

Random asymmetric coupling: gaps and self-loops.— We now exploit random interactions, where c_{ij} and c_{ji} are sampled independently. For any value of H, each isolated element has one stable phase, or two within the hysteretic range. Without interactions, stable states can be easily formed by combining stable elements. However, interactions make the switching fields dependent on the collective state, effectively randomizing stability ranges and creating *gaps*, ranges of H where no state is stable.

We find two related scenarios where interactions lead to self-loops. We consider state S going unstable by the driving crossing a critical value H^c. In the first scenario, H^c lies in a gap, and the system gets inevitably trapped in a self-loop. In the second, the system also gets trapped, despite the presence of other stable states at $H = H^c$.

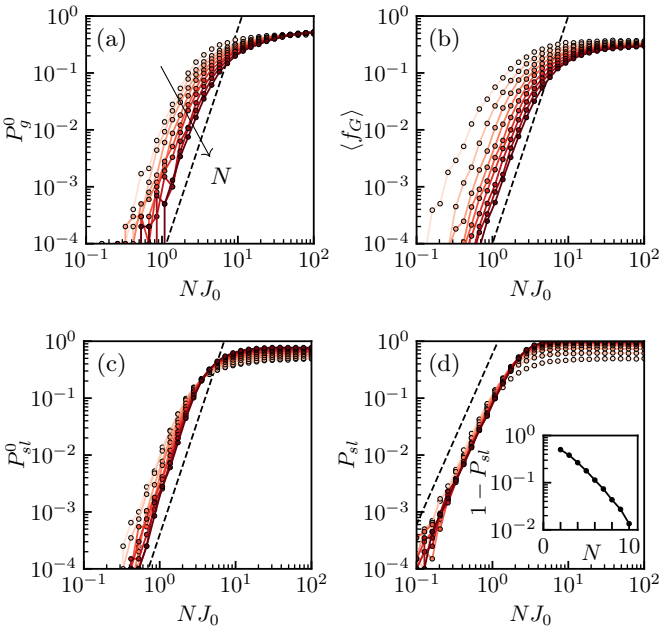

FIG. 2: Statistical measures for gaps and self-loops scale when plotted as function of NJ_0 (10^5 samples; color from light to dark as N increases from 2 to 10). (a) Probability P_g^0 of finding a gap at $H = 0$ (dashed line indicates slope 4). (b) Averaged fraction of gaps f_G, where f_G is defined as the ratio of the size of intervals where no stable states exist divided by $H^+(--\dots) - H^-(++\dots)$ (dashed line indicates slope 4). (c) Probability P_{sl}^0 of finding at least one self-loops at $H = 0$ (dashed line indicates slope 4). (d) Probability P_{sl} of finding at least one self-loop for any value of H (dashed line indicates slope 3). Inset: The probability to be self-loop free, $1 - P_{sl}$, decays to zero exponentially with N for large couplings ($NJ_0 = 10^2$).

To investigate the statistics of gaps and self-loops, we sample the model using an event-driven algorithm [5]. We consider collections of hysterons with thresholds in a compact range [5, 8, 30], and for the bare switching fields, we flatly sample the midpoints $h_i^c = (h_i^+ + h_i^-)/2$ from the interval $[-1, 1]$ and the interaction coefficients c_{ij} from $[-J_0, J_0]$. Unless noted otherwise, we flatly sample the spans $\sigma_i = h_i^+ - h_i^-$ from $[0, 0.5]$.

We find that the probability P_g^0 of a gap, meaning the absence of a stable state at $H = 0$, and the fraction of gaps f_G, both increase as power laws when $NJ_0 \ll 1$ (Figs. S3a-b). For $NJ_0 \gg 1$, they saturate at significant values. The probability that states have a finite stability range decreases exponentially with N: for large N, stable states become rare, prohibiting statistical studies of transitions (Supplemental Material).

Gaps imply self-loops, but self-loops can also occur without gaps: the probability of a self-loop occurring for a random state at $H = 0$, P_{sl}^0, is larger than the corresponding gap probability P_g^0 (Fig. S3c and Supplemental Material). Similarly, we calculated the probability of observing a self-loop at any value of H, P_{sl}, by starting from every stable state, in/decreasing H, and checking

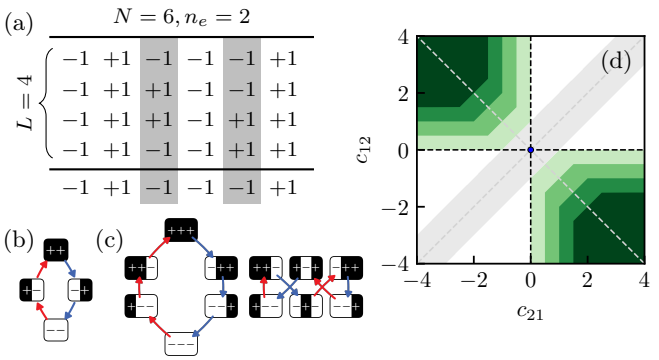

FIG. 3: (a) Example of the state evolution in a self-loop ($N = 6, L = 4, n_e = 2$). (b) The only fundamental $L = 4$ self-loop (up/down transitions: red/blue arrows). (c) Two out of six possible $L = 6$ fundamental self-loops — these are the only ones realizable with WA interactions (see Table I). (d) Location of $L = 4$ self-loops for $N = 2$ hysterons, where we fix $\Delta h^c = 1$ and vary the minimal span σ from 0 to 3 in steps of 1 (light to dark green).

whether the ensuing transition yields at least one self-loop. We find that P_{sl} exceeds the corresponding fraction of gaps, and approaches one in large, strongly coupled systems (Fig. S3d; Supplemental Material). This dominance of self-loops is robust; hysterons with fixed spans $\sigma_i = 0.5$ and binary spins where $\sigma_i = 0$ also have $P_{sl} \to 1$ in the large coupling limit (Supplemental Material) [32–35]. Hence, self-loops, incompatible with the dissipative systems we aim to model, are unavoidable for random interactions, and for large systems completely overwhelm the response.

Proliferation of self-loops.— Each self-loop is associated with a set of linear inequalities of $(h_i^{\pm}, c_{ij})$, and occurs in a polytope in parameter space [5, 21, 30, 31]. By identifying all potential self-loops, one could, in principle, determine all corresponding polytopes; the complement of their union is then free of self-loops. However, the number of self-loops grows extremely rapidly with N.

We characterize each self-loop by its length L and by the $n_e \leq N$ elements that are involved (Fig. S9a). We focus on *fundamental* loops, which are defined as the unique loops that involve all elements ($n_e = N$) up to permutations (i.e., the self-loop $(--)\to(-+)\to(++)\to(+-)\to\dots$ is equivalent to the loop in Fig. S9b). We determine the potential number of fundamental loop structures, $M(n_e, L)$, from the combinatorics of flip sequences, and calculate the number of realizable loops with pairwise interactions, $M_R(n_e, L)$ (Supplemental Material). Both grow rapidly with n_e and L (Table I). In particular, for the shortest fundamental loops, $M(n_e, L = 2n_e)$ grows as $1, 6, 56, 796, \dots$ for $n_e = 2, 3, 4, 5, \dots$ (Figs. S9-b and c for $n_e = 2, 3$), and our data suggests that each of these is realizable. The number of actual self-loops and polytopes grows even faster with N. Introducing n_e elements into a larger group of N elements, and including permutations, maps each fundamental loop to a significantly larger number of actual loops and polytopes, fueling a further combinatorial explosion.

Lenient and strict strategies.— The proliferation of the number, length, and complexity of self-loops for large N makes deriving explicit and sharp conditions that identify all self-loops unfeasible. We thus first introduce a lenient strategy that fully eliminates the shortest self-loops and suppresses—though not completely eliminates—longer ones. We then define strict ensembles that entirely eliminate self-loops of any length but are overly restrictive.

L/n_e	2	3	4	5
4	1/1/0	–	–	–
6	–	6/6/2	–	–
8	–	2/0/0	56/56/24	–
10	–	–	176/114/4	796/796/376
12	–	–	420/145/1	9028/x/x
14	–	–	448/48/0	76640/x/x
16	–	–	112/4/0	535584/x/x

Table I: Numbers of fundamental self-loops of size L involving n_e elements. Note that $4 \leq L \leq 2^N$ and $\log_2 L \leq n_e \leq L/2$, as each element undergoes an even number of flips; loops with n_e elements can visit at most 2^{n_e} states; and self-loops of size 2 are excluded by $h_i^+ \geq h_i^-$ (Supplemental Material). The numbers in each box represents $M(n_e, L)$, $M_R(n_e, L)$, and $M_W(n_e, L)$, respectively. Note that the number of longest fundamental loops, $M(n_e, L = 2^{n_e})$, are given by the number of directed Hamiltonian cycles in the binary n_e-cube $(1, 2, 112, 15109096, \dots$ for $n_e = 2, 3, 4, 5, \dots)$ [45, 46].

Lenient strategy: weak asymmetry.— Short ($L = 4$) loops are sufficiently simple that we can derive their polytope conditions easily. First, for the simplest case of $L = 4$ self-loops for two spins, we find that a gap of size $|\Delta c| - |\Delta h^c|$ opens up when $c_{12}c_{21} < 0$ and $|\Delta c| > |\Delta h^c|$, where $\Delta c := c_{12} - c_{21}$ and $\Delta h^c := h_2^c - h_1^c$. These conditions are sufficient and necessary for the emergence of a self-loop. For two hysterons, the lower bound of the spans σ_i is crucial: if it is zero, the same conditions apply, but if it is positive, there is a larger range in parameter space that is guaranteed to be free of $L=4$ self-loops (Fig. S9d). Finally, we can extend these conditions to arbitrary N; as for $L = 4$ self-loops only two elements i and j are involved, we can prohibit short self-loops by requiring $c_{ij}c_{ji} \geq 0$ for all pairs (i, j) (For details, Supplemental Material).

We thus introduce the notion of weak asymmetry (WA): $c_{ij}c_{ji} \geq 0$ for all pairs (i, j). Not only does WA eliminates $L = 4$ self-loops, but it also suppresses the number of longer self-loops that are realizable (Table I, and Supplemental Material). Statistical sampling reveals that WA is an effective strategy to suppress self-loops. In particular, $P_{sl}^0 \to 0$ for large N, allowing to sample individual transitions, although P_{sl} slowly grows with N: the combinatorial possibilities of finding a self-loop dominates in large systems (Supplemental Material). Nevertheless, for intermediate N, WA strongly suppresses self-loops, e.g., $P_{sl} \approx 14\%$ for large couplings and $N = 10$. Hence, WA strictly prohibits short self-loops and sup-

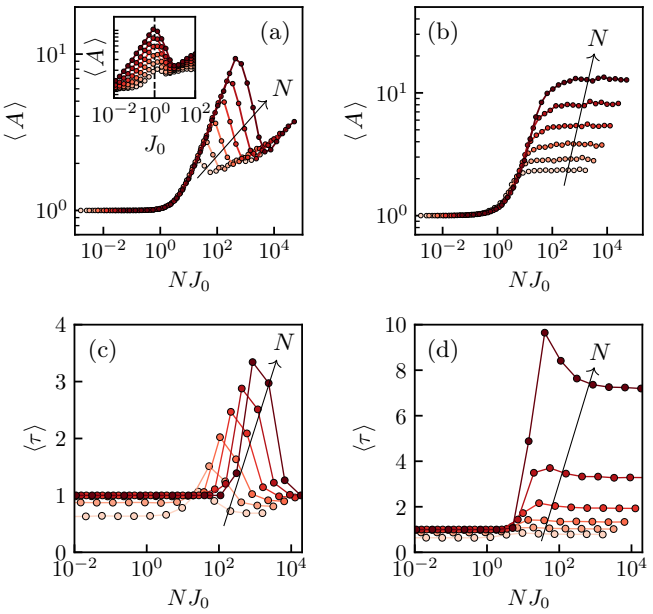

FIG. 4: Simulations of large systems of coupled hysterons in the constant-columns (left) and symmetric (right) ensembles ($N = 16, 32, \ldots, 512$ for increasingly dark colors). (a-b) Ensemble averaged avalanche size $\langle A \rangle$. To determine these, we initialize the system at a stable state S^0 at $H = 0$, increase H, and measure the number of flips before the system settles on a stable state. (c-d) Ensemble averaged transient $\langle \tau \rangle$, where τ is the number of cyclic drive cycles after which the system reaches a periodic orbit (Supplemental Material).

presses longer self-loops.

Strict ensembles.— We now present ensembles of asymmetric interactions which strictly prohibit self-loops. First, if all interactions are positive ($c_{ij} \geq 0$), avalanches exhibit monotonic evolution of the magnetization $m := \Sigma s_i$, thus prohibiting self-loops (Appendix B). If all interactions are negative, and either $c_{ik} = -d_k$ (constant-columns) or $c_{ki} = -d_k$ (constant-rows), where $d_k \geq 0$, self-loops are also prohibited. In the former case, the interactions prohibit scrambling [12], which in turn prohibits self-loops (Appendix C); in the latter case, the interactions only allow avalanches of length two, too short to form a self-loop (Appendix D and Supplemental Material). We note that the statistics of, e.g., avalanches and self-loops drastically depends on the dynamical rule in all these ensembles. In particular, when race conditions are not allowed [12, 21, 31], constant-columns interactions restrict the avalanche size $A \leq 2$, whereas flipping the most (or least) unstable elements leads to much larger A (Fig. 4-a); moreover, flipping all unstable elements simultaneously instead of only the most unstable one leads to a dominance of $L = 2$ self-loops for symmetric, constant-columns and constant-rows interactions (see Supplemental Material).

The strictly self-loop-free ensembles allow us to study the statistics of unprecedentedly large systems of interacting hysterons, including the distributions of avalanche sizes A, transient times τ, and multiperiodicities T of orbits under cyclic drive (Fig. 4; see Supplemental Material). We find that these significantly depend on the ensemble, e.g., avalanches and transients are shorter in the constant-columns ensemble than in the symmetric ensemble, and their dependence on NJ_0 is qualitatively different.

Discussion.— Self-loops are forbidden in dissipative systems and an important feature of active systems [41, 47]. As the parameter regions where self-loops occur form a vast cloud of complex polytopes, it is unlikely that simple, precise expressions can be found to distinguish regions with and without self-loops. We introduce lenient and strict ensembles, and note that the symmetric, WA, strictly positive, and constant-columns interactions can all be realized experimentally [5, 12, 26, 28] (Supplemental Material).

Our work suggests multiple directions for future research. First and foremost is the need to explore explicit mappings from physical models to hysteron models. Different ensembles and dynamical rules result in distinct statistical properties (Fig. 4). Furthermore, since well-behaved dissipative models are inherently self-loop free, the dynamical rules and interaction ensembles associated with them must also ensure self-loop free behavior. Indeed, for networks of overdamped bistable springs [7, 12, 26, 48], such a mapping yields strongly asymmetric interactions without self-loops. Hence, physical mappings are a compelling subject for further investigation. Second, self-loops and multiperiodic responses under cyclic driving [5] have links that can be revealed using the recently introduced concept of the transition scaffold [31]. In particular, we suggest that multiperiodic responses (such as an orbit of period $T = 3$ as compared to the period of the driving) can be constructed starting from its corresponding self-loop (such as Fig. S9c-right). Finally, prohibiting self-loops is mirrored in recent works that aim to understand the emergence of oscillating dynamics through non-reciprocal phase transitions, and we suggest investigating other interaction ensembles (like WA, constant-columns, or otherwise derived from an underlying model) in this context [40, 41, 47].

Acknowledgments

PB and MvH acknowledge funding from European Research Council Grant ERC-101019474. We thank Dor Shohat, Yoav Lahini, Corentin Coulais and Menachem Stern for discussions.

Appendix A: Systematic convergence for symmetric interactions.

Here we show that symmetric interactions yield transitions that lower a Lyapounov function, first focusing on spins (for which $h_i^+ = h_i^- = h_i^c$) following standard approaches [37, 49], and then extending the result to hysterons. Consider an initial state S^0 and a value of the drive H such that element p is unstable, which implies:

- $H > h_p^c - \sum_{j\neq p} c_{pj} s_j^0$, if $s_p^0 = -1$,
- $H < h_p^c - \sum_{j\neq p} c_{pj} s_j^0$, if $s_p^0 = 1$,

which can be rewritten as:

$$s_p^0 \left(H - h_p^c + \sum_{j\neq p} c_{pj} s_j^0 \right) < 0 \ . \tag{A1}$$

Let us now introduce the function V, reminiscent of a Sherrington-Kirkpatrick model with random fields:

$$\begin{aligned} V(\boldsymbol{s}) &= -\sum_i \left[s_i (H - h_i^c) + \frac{1}{2} \sum_{j\neq i} c_{ij} s_i s_j \right] , \\ &= -\sum_i s_i (H - h_i^c) - \frac{1}{2} \sum_i \sum_{j\neq i} c_{ij} s_i s_j , \end{aligned} \tag{A2}$$

where the first and second term on the r.h.s. of Eq. (A2) can be seen as a field and interaction term. We aim to compute $\Delta V = V(S^1) - V(S^0)$, where S^1 and S^0 are the state before and after snapping element p, i.e. $s_{i\neq p}^1 = s_{i\neq p}^0$, and $s_p^1 = -s_p^0$. Clearly, the terms with elements different than p will not contribute to ΔV, and by splitting the sums accordingly, we obtain:

$$\Delta V = -s_p^1 (H - h_p^c) + s_p^0 (H - h_p^c) - \frac{1}{2} \left(\sum_{i\neq p} c_{ip} s_i s_p^1 + \sum_{j\neq p} c_{pj} s_p^1 s_j - \sum_{i\neq p} c_{ip} s_i s_p^0 - \sum_{j\neq p} c_{pj} s_p^0 s_j \right) , \tag{A3}$$

which can be simplifed to:

$$\Delta V = 2 s_p^0 \left[(H - h_p^c) + \frac{1}{2} \sum_{j\neq p} (c_{jp} + c_{pj}) \, s_j \right] , \tag{A4}$$

where we repeatedly use that for $j \neq p$, $s_j^0 = s_j^1 =: s_j$ For the case of symmetric interactions, i.e. $c_{jp} = c_{pj}$, we find:

$$\Delta V = 2 s_p^0 \left[(H - h_p^c) + \sum_{j\neq p} c_{pj} s_j \right] . \tag{A5}$$

Inserting the instability condition for element p, Eq. (A1) yields $\Delta V < 0$. Therefore, the function V is strictly decreasing for each single flip, which implies that the system cannot be trapped in a self-loop and must always evolve toward a stable state. Note the importance of the factor 1/2 in Eq. (A2) in order to obtain the final result. This demonstration can be extended to finite span hysterons, by explicitly making the distinction between hysterons with positive and negative phase, and their respective thresholds, producing Eq. 2 of the main text.

Appendix B: Positive interactions.

In this section, we show that for positive (ferromagnetic) interactions, i.e. $c_{ij} \geq 0$, the system cannot get trapped into a self-loop. A self-loop is a cyclic avalanche: the system must come back to a previously visited unstable state. However, for positive interactions, each step in an avalanche 'goes in the same direction', i.e., the magnetization $m := \sum_i s_i$ evolves monotonously [21, 50]. This prevents avalanches from revisiting earlier states, thus prohibiting self-loops, irrespective of the specific rule used to resolve race conditions (Supplemental Material).

Appendix C: Constant-columns interactions.

We now clarify why constant-columns ($c_{ik} = -d_k$, $d_k \geq 0$) define a self-loop-free interaction ensemble. First, for negative (antiferromagnetic) interactions, avalanches (including self-loops) must be composed of alternating up/down transitions [21]. For $L \geq 6$, such self-loops exist (Fig. S9-c, and Supplemental Material). However, all such self-loops violate loop-RPM, which requires scrambling: the ordering of the switching fields must be state-dependent [21]. Constant-columns interactions do not allow for scrambling [12], therefore this ensemble strictly prevents all self-loops.

Appendix D: Constant-rows interactions

We now show that in the constant-rows ensemble ($c_{ki} = -d_k$, $d_k \geq 0$), avalanches consist of at most two hysteron flips, which is too short to allow self-loops. Without loss of generality, we consider an up avalanche initiated from state S^0 by an increase of H up to $H_p^+(S^0)$, triggering the flipping of hysteron p from $s_p = -1$ to $s_p = 1$, and leading to state S^1. Since we have negative interactions, avalanches must be composed of alternating up/down transitions, so that the next step would be the flipping of hysteron q from $s_q = 1$ to $s_q = -1$ leading to state S^2. To show that S^2 is stable to additional up

flipping events, we first show that $H_i^+(S^0) = H_i^+(S^2)$ for $i \neq p, q$. Using that in this ensemble $c_{ip} = c_{iq}$, and that $s_p^0 = -1$ and $s_q^0 = 1$, we find that

$$H_{i\neq p,q}^+(S^0) = h_i^+ - \sum_j c_{ij} s_j^0 \quad \text{(D1)}$$

$$= h_i^+ - \sum_{j\neq p,q} c_{ij} s_j^0 - c_{ip} s_p^0 - c_{iq} s_q^0 \quad \text{(D2)}$$

$$= h_i^+ - \sum_{j\neq p,q} c_{ij} s_j^0 \ . \quad \text{(D3)}$$

Similarly, using that $s_p^2 = 1$ and $s_q^2 = -1$, we find that

$$H_{i\neq p,q}^+(S^2) = h_i^+ - \sum_{j\neq p,q} c_{ij} s_j^2 \ , \quad \text{(D4)}$$

and as $s_{j\neq p,q}^2 = s_{j\neq p,q}^0$, we conclude that $H_i^+(S^0) = H_i^+(S^2)$ for $i \neq p, q$. Since in state S_0 all hysterons $i \neq p, q$ are stable, they are also stable in state S^2. Moreover, both hysterons p and q are stable in state S^2 at $H = H_p^+(S^0)$: indeed $H_p^-(S^2) = H_p^+(S^0) - \sigma_p - 2d_p < H_p^+(S^0)$, and hysteron q just flipped. Therefore, the longest possible avalanche in this interaction ensemble consists of two steps. By the same argument, this result also holds for other race conditions which involve flipping hysterons one by one (Supplemental Material).

[1] F. Preisach, Zeitschrift für physik **94**, 277 (1935).
[2] N. C. Keim, J. D. Paulsen, Z. Zeravcic, S. Sastry, and S. R. Nagel, Reviews of Modern Physics **91**, 035002 (2019).
[3] J. D. Paulsen and N. C. Keim, Proceedings of the Royal Society A **475**, 20180874 (2019).
[4] C. W. Lindeman and S. R. Nagel, Science Advances **7**, eabg7133 (2021).
[5] N. C. Keim and J. D. Paulsen, Science Advances **7**, eabg7685 (2021).
[6] T. Jules, A. Reid, K. E. Daniels, M. Mungan, and F. Lechenault, Physical Review Research **4**, 013128 (2022).
[7] D. Shohat, D. Hexner, and Y. Lahini, Proceedings of the National Academy of Sciences **119**, e2200028119 (2022).
[8] N. C. Keim and D. Medina, Science Advances **8**, eabo1614 (2022).
[9] J. D. Paulsen and N. C. Keim, arXiv preprint arXiv:2405.08158 (2024).
[10] H. Bense and M. van Hecke, Proceedings of the National Academy of Sciences **118**, e2111436118 (2021).
[11] L. J. Kwakernaak and M. van Hecke, Physical Review Letters **130**, 268204 (2023).
[12] J. Liu, M. Teunisse, G. Korovin, I. R. Vermaire, L. Jin, H. Bense, and M. van Hecke, Proceedings of the National Academy of Sciences **121**, e2308414121 (2024).
[13] D. Melancon, A. E. Forte, L. M. Kamp, B. Gorissen, and K. Bertoldi, Advanced Functional Materials **32**, 2201891 (2022).
[14] A. Meeussen and M. van Hecke, Nature **621**, 516 (2023).
[15] M. Brandenbourger, C. Scheibner, J. Veenstra, V. Vitelli, and C. Coulais, arXiv preprint arXiv:2108.08837 (2021).
[16] J. Veenstra, O. Gamayun, X. Guo, A. Sarvi, C. V. Meinersen, and C. Coulais, Nature **627**, 528 (2024).
[17] L. M. Kamp, M. Zanaty, A. Zareei, B. Gorissen, R. J. Wood, and K. Bertoldi, arXiv preprint arXiv:2409.03737 (2024).
[18] M. Mungan, S. Sastry, K. Dahmen, and I. Regev, Physical review letters **123**, 178002 (2019).
[19] M. Mungan and M. M. Terzi, in *Annales Henri Poincaré*, Vol. 20 (Springer, 2019) pp. 2819–2872.
[20] M. M. Terzi and M. Mungan, Physical Review E **102**, 012122 (2020).
[21] M. van Hecke, Physical Review E **104**, 054608 (2021).
[22] G. Puglisi and L. Truskinovsky, Journal of the Mechanics and Physics of Solids **48**, 1 (2000).
[23] A. Nicolas, E. E. Ferrero, K. Martens, and J.-L. Barrat, Reviews of Modern Physics **90**, 045006 (2018).
[24] D. Kumar, S. Patinet, C. E. Maloney, I. Regev, D. Vandembroucq, and M. Mungan, The Journal of Chemical Physics **157** (2022).
[25] D. Kumar, M. Mungan, S. Patinet, and D. Vandembroucq, arXiv preprint arXiv:2409.07621 (2024).
[26] D. Shohat and M. van Hecke, arXiv preprint arXiv:2409.07804 (2024).
[27] J. Ding and M. van Hecke, The Journal of Chemical Physics **156** (2022).
[28] J. D. Paulsen, arXiv preprint arXiv:2409.07726 (2024).
[29] N. C. Keim, J. Hass, B. Kroger, and D. Wieker, Physical Review Research **2**, 012004 (2020).
[30] C. W. Lindeman, T. R. Jalowiec, and N. C. Keim, arXiv preprint arXiv:2306.07177 (2023).
[31] M. H. Teunisse and M. van Hecke, arXiv preprint arXiv:2404.11344 (2024).
[32] H. Gutfreund, J. Reger, and A. Young, Journal of Physics A: Mathematical and General **21**, 2775 (1988).
[33] K. Nutzel and U. Krey, Journal of Physics A: Mathematical and General **26**, L591 (1993).
[34] H. Eissfeller and M. Opper, Physical Review E **50**, 709 (1994).
[35] S. Hwang, V. Folli, E. Lanza, G. Parisi, G. Ruocco, and F. Zamponi, Journal of Statistical Mechanics: Theory and Experiment **2019**, 053402 (2019).
[36] S. Kirkpatrick and D. Sherrington, Physical Review B **17**, 4384 (1978).
[37] J. J. Hopfield, Proceedings of the national academy of sciences **79**, 2554 (1982).
[38] A. Crisanti and H. Sompolinsky, Physical Review A **36**, 4922 (1987).
[39] D. Panchenko, *The sherrington-kirkpatrick model* (Springer Science & Business Media, 2013).
[40] M. Fruchart, R. Hanai, P. B. Littlewood, and V. Vitelli, Nature **592**, 363 (2021).
[41] G. G. Lorenzana, A. Altieri, G. Biroli, M. Fruchart, and V. Vitelli, arXiv preprint arXiv:2408.17360 (2024).
[42] C. Coulais, D. Sounas, and A. Alu, Nature **542**, 461 (2017).
[43] G. Parisi, Fractals **11**, 161 (2003).

[44] M. B. Jesi, *Spin Glasses: Criticality and Energy Landscapes* (Springer, 2016).
[45] D. E. Knuth, in *The art of computer programming: fundamental algorithms* (1975) pp. 634–634.
[46] M. Deza and R. Shklyar, arXiv preprint arXiv:1003.4391 (2010).
[47] Y. Avni, M. Fruchart, D. Martin, D. Seara, and V. Vitelli, arXiv preprint arXiv:2409.07481 (2024).
[48] D. Shohat, Y. Friedman, and Y. Lahini, Nature Physics **19**, 1890 (2023).
[49] D. J. C. MacKay, *Information Theory, Inference, and Learning Algorithms* (Cambridge University Press, Cambridge, UK, 2003) available online at `http://www.inference.org.uk/itprnn/book.pdf`.
[50] J. P. Sethna, K. Dahmen, S. Kartha, J. A. Krumhansl, B. W. Roberts, and J. D. Shore, Physical Review Letters **70**, 3347 (1993).

Supplemental Material: Proliferation and prohibition of self-loops in ensembles of interacting binary elements

Paul Baconnier[1], Margot H. Teunisse[1,2] and Martin van Hecke[1,2]

[1] *AMOLF, 1098 XG Amsterdam, The Netherlands.*
[2] *Huygens-Kamerlingh Onnes Laboratory, Leiden University, 2300 RA Leiden, The Netherlands.*

In the main manuscript, we investigate the root causes and statistics of self-loops in ensembles of interacting binary elements, and we find several strict ensembles that are completely free of self-loops. In this document, we first elaborate on the conditions under which a self-loop emerges in the transition-graph shown in Fig. 1 of the main text. In Secs. 2 and 3, we discuss the probability of race conditions and the probability that a given state has a finite stability range as a function of coupling strength, for randomly-coupled spins and hysterons. In Secs. 4 and 5, we provide numerical evidence the problem of overwhelming self-loops is similar for spins instead of hysterons, and for ensembles of hysterons with equal spans. In Sec. 6, we further analyze the relationship between gaps and self-loops. In Sec. 7, we provide numerical evidence that self-loops also overwhelm the response of large systems in the case of weakly asymmetric interactions. In Sec. 8, we derive the conditions to prevent $L = 4$ self-loops for $N = 2$ spins and $N = 2$ hysterons with equal spans, and sample $L = 4$ self-loops for large N. In Sec. 9, we provide physical illustrations for the different classes of well-behaved models. In Sec. 10, we analyze the role of the different race conditions rules in the different families of models. In Sec. 11, we give details on the algorithm to generate all possible self-loops, and illustrate the different possible self-loop structures for different sizes L. Finally, in Sec. 12, we discuss numerical simulations of large systems of self-loop-free models.

1: Conditions for a self-loop of size 4 in the general model

In this section, we elaborate on the conditions under which a self-loop emerges in the graph represented in Fig. 1 of the main text. A sufficient condition for self-loops is that H is in a range where all the states S^0, S^1, S^2 and S^3 are unstable. This situation is realized when H is larger than the two up switching fields $H^+(S^0)$ and $H^+(S^1)$, smaller than the two down switching fields $H^-(S^2)$ and $H^-(S^3)$, and when both $H^+(S^0)$ and $H^+(S^1)$ are smaller than $H^-(S^2)$ and $H^-(S^3)$.

Starting from a stable state and driving the system up to instability, what are the conditions under which the transition triggers a self-loop? In this case, we evaluate the possibility for a self-loop for H immediately above (below) the up (down) switching field of a given state. For each of the four possible starting states, we can write down the inequalities needed so that the self-loop shown on Fig. 1 of the main text is realized:

- **State** S^0: this state becomes unstable as soon as $H > H^+(S^0)$, and a self-loop emerges at instability when:

$$\begin{aligned} &H^+(S^1) < H^+(S^0), \\ &H^-(S^2) > H^+(S^0), \\ &H^-(S^3) > H^+(S^0), \end{aligned} \tag{S1}$$

  where each relationship enforces that a given state of the loop is unstable. Hence, a self-loop is triggered when: $H^+(S^1) < H^+(S^0) < \big(H^-(S^2), H^-(S^3)\big)$ (see caption of Fig. 1 of the main text).

- **State** S^1: this state becomes unstable as soon as $H > H^+(S^1)$, and a self-loop emerges at instability when:

$$\begin{aligned} &H^+(S^0) < H^+(S^1), \\ &H^-(S^2) > H^+(S^1), \\ &H^-(S^3) > H^+(S^1). \end{aligned} \tag{S2}$$

  This produces the condition: $H^+(S^0) < H^+(S^1) < \big(H^-(S^2), H^-(S^3)\big)$.

- **State** S^2: this state becomes unstable as soon as $H < H^-(S^2)$, and a self-loop emerges at instability when:

$$\begin{aligned} &H^-(S^3) > H^-(S^2), \\ &H^+(S^0) < H^-(S^2), \\ &H^+(S^1) < H^-(S^2). \end{aligned} \tag{S3}$$

Yielding: $\big(H^+(S^0), H^+(S^1)\big) < H^-(S^2) < H^-(S^3)$.

- **State** S^3: this state becomes unstable as soon as $H < H^-(S^3)$, and a self-loop emerges at instability when:

$$\begin{aligned} &H^-(S^2) > H^-(S^3), \\ &H^+(S^0) < H^-(S^3), \\ &H^+(S^1) < H^-(S^3). \end{aligned} \tag{S4}$$

Yielding: $\big(H^+(S^0), H^+(S^1)\big) < H^-(S^3) < H^-(S^2)$.

2: Race conditions

Here, we investigate the probability of race conditions for collections of spins ($\sigma_i = 0$), hysterons (σ_i flatly sampled from $[0, 0.5]$), and hysterons with equal spans ($\sigma_i = 0.5$).

When a state S^0 becomes unstable and one of the hysterons flips to produce state S^1, the number of unstable hysterons in S^1 can be either zero (S^1 is stable), one, or more than one. If more than one hysteron is unstable, this causes a race condition. We calculate the race-condition probability P_{RC} – the probability of more than one hysteron being unstable in state S^1 – by selecting a state S^0 that is stable at $H = 0$, increasing H past $H^+(S^0)$, and investigating the number of unstable hysterons of S^1 at $H = H^+(S^0)$. We find that P_{RC} increases as $(NJ_0)^2$ for $NJ_0 \ll 1$, and saturates at a significant value that increases towards 1 for large N for $NJ_0 \gg 1$ (Figs. S1). We observe only minor differences between spins, hysterons, and hysterons with equal spans.

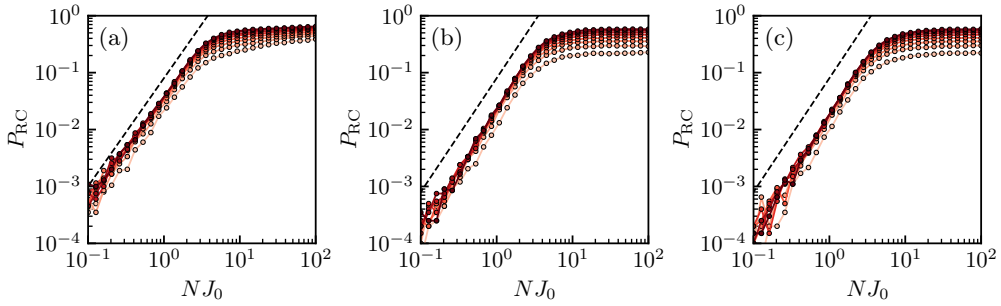

FIG. S1: **Statistics of race conditions for randomly-coupled two-states elements.** Probability P_{RC} of race conditions (ensemble of 2×10^4 transitions $S^0 \to S^1$), for an initial state S^0 stable at $H = 0$; the black dashed line represents the slope 2. Markers are color coded from light to dark red as N increases, with $N \in [2, 3, 4, 5, 6, 7, 8, 9, 10]$. (a) Spins ($\sigma_i = 0$). (b) Hysterons ($\sigma_i$ flatly sampled from $[0, 0.5]$). (c) Hysterons with equal spans ($\sigma_i = 0.5$).

3: Number of stable states

In this section, we measure the probability that a given state has a finite stability range for collections of spins ($\sigma_i = 0$), hysterons (σ_i flatly sampled from $[0, 0.5]$), and hysterons with equal spans ($\sigma_i = 0.5$).

Independently of the microscopic hysteresis and coupling strength, the probability P_s that a random state S among the 2^N possible states is stable for some value of the driving H, i.e. $H^+(S) > H^-(S)$, asymptotes to 0 for large N. Indeed, for spins, it is easy to show that there always exists only $N + 1$ potentially stable states, so that $P_s = P_{\mathrm{spins}} = (N + 1)/2^N$ (Fig. S2-a).

For hysterons and hysterons with equal spans, we find that P_s asymptotes toward P_{spins} in the large coupling limit, i.e., $NJ_0 \gg 1$ (Figs. S2-b and c). However, in the small coupling limit, P_s is larger than P_{spins}. In this case, P_s is dictated by the statistics of the Preisach graphs that are sampled, which is itself dictated by the statistics of the different orderings of the switching fields $h_i^{\pm}$. Interestingly, in the case of hysterons with equal spans, the Preisach graphs which are sampled generally contain more stable states. Note that in all case, P_s still asymptotes to 0 even in the small coupling limit, but slower than in the case of spins.

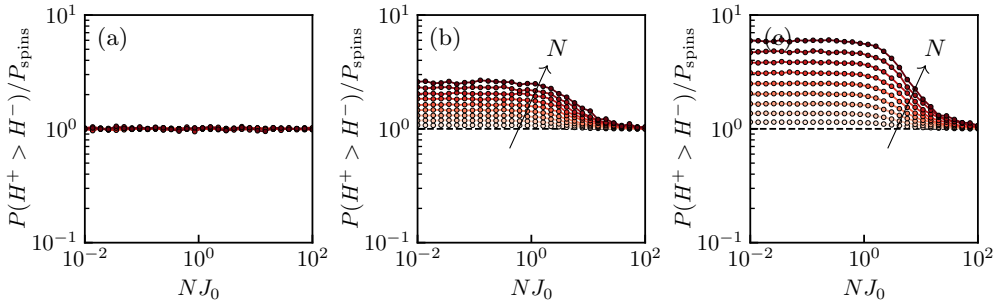

FIG. S2: **Fraction of potentially stable states.** Probability that a randomly chosen state S has a finite stability range; scaled by $P_{\rm spins} = (N+1)/2^N$. Markers are color coded from light to dark red as N increases, with $N \in [2, 3, 4, 5, 6, 7, 8, 9, 10]$. (a) Spins ($\sigma_i = 0$). (b) Hysterons ($\sigma_i$ flatly sampled from $[0, 0.5]$). (c) Hysterons with equal spans ($\sigma_i = 0.5$).

4: Case of binary spins

In this section, we reproduce the simulations of Fig. 2 of the main text, focusing on the case of randomly-coupled spins, i.e. $\sigma_i = 0$ for all the elements (Figs. S3).

Let us focus on the similarities between spins and hysterons with distributed spans. In both cases, the statistical weight of gaps increases as a power law for $NJ_0 \ll 1$, and saturates toward a significant value for $NJ_0 \gg 1$ (Figs. S3-a and b). Moreover, the probability of finding at least one self-loop for any H increases as a power law for $NJ_0 \ll 1$, and saturates toward a constant value for $NJ_0 \gg 1$ (Fig. S3-d), which asymptotes to 1 as N increases (Fig. S3-d, inset). Therefore, the response of large, strongly coupled systems of spins is dominated by self-loops.

There are however subtle differences with the case of hysterons. In particular, for spins, all observables grow slower with NJ_0 but are bigger than for hysterons for $NJ_0 \ll 1$ (there are more gaps and self-loops for spins than for hysterons in the small coupling limit). Also, for $NJ_0 \gg 1$, self-loops are more likely with spins than with hysterons: for $N = 10$ and in the large coupling limit ($NJ_0 = 10^2$), 99.8% of instances exhibit at least one self-loop for spins, while the probability is 98.5% for hysterons. This is expected given that microscopic hysteresis contributes to preventing self-loops.

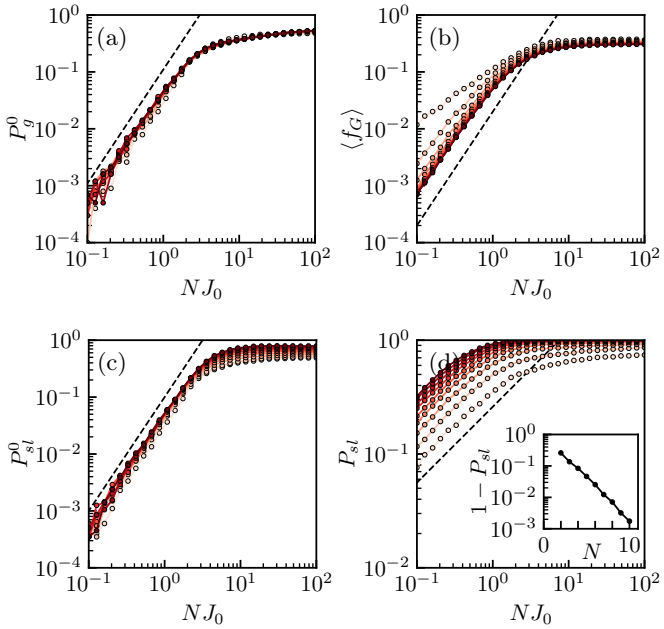

FIG. S3: **Overwhelming self-loops for randomly-coupled spins.** Statistical measures for gaps and self-loops scale when plotted as function of NJ_0 and dominate for $NJ_0 \gg 1$ (10^5 samples; color from light to dark as N increases from 2 to 10). (a) Probability P_g^0 of finding a gap at $H = 0$ (dashed line indicates slope 2). (b) Fraction of gaps f_g, defined as the mean of the ratio of the size of intervals where no stable states exist divided by $\left[H^+(-\cdots-), H^-(+\cdots+)\right]$ (dashed line indicates slope 2). (c) Probability P_{sl}^0 of self-loops at $H = 0$ (dashed line indicates slope 2). (d) Probability P_{sl} of finding at least one self-loop for any value of H (dashed line indicates slope 2/3). Inset: The probability to be self-loop free, $1 - P_{sl}$, decays to zero exponentially with N for large couplings ($NJ_0 = 10^2$).

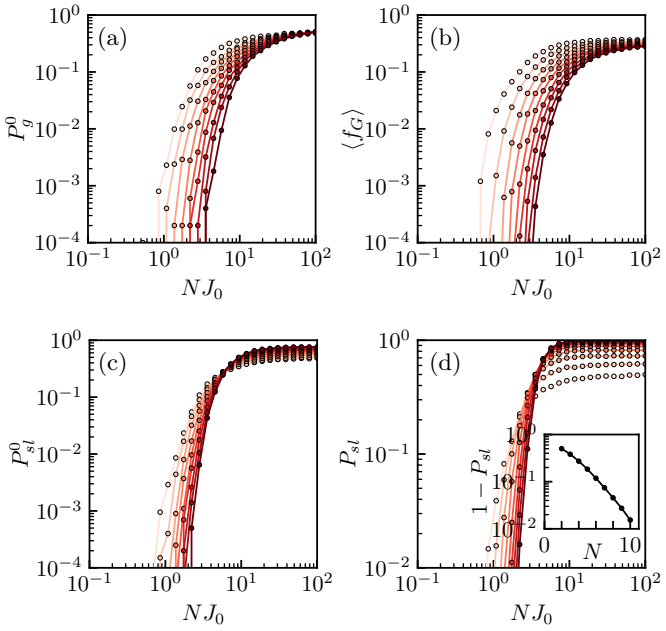

FIG. S4: **Overwhelming self-loops for randomly-coupled hysterons with equal spans.** Statistical measures for gaps and self-loops scale when plotted as function of NJ_0 and dominate for $NJ_0 \gg 1$ (10^5 samples; color from light to dark as N increases from 2 to 10). (a) Probability P_g^0 of finding a gap at $H = 0$. (b) Fraction of gaps f_g, defined as the mean of the ratio of the size of intervals where no stable states exist divided by $\left[H^+(-\cdots-), H^-(+\cdots+)\right]$. (c) Probability P_{sl}^0 of self-loops at $H = 0$. (d) Probability P_{sl} of finding at least one self-loop for any value of H. Inset: The probability to be self-loop free, $1 - P_{sl}$, decays to zero exponentially with N for large couplings ($NJ_0 = 10^2$).

5: Case of hysterons with equal spans

In this section, we reproduce the simulations of Fig. 2 of the main text, focusing on the case of randomly-coupled hysterons with equal spans, i.e. $\sigma_i = 0.5$ for all the elements (Figs. S4).

We find that the probability of finding at least one self-loops for any H saturates toward a constant value for $NJ_0 \gg 1$ (Fig. S4-d), which asymptotes to 1 as N increases (Fig. S4-d, inset). However, in the case of hysterons with equal spans, we find that all observables seem to have a lower cutoff in NJ_0 below which no gaps or self-loops exist. This is expected given the physics of self-loops for $N = 2$ hysterons (see Fig. 3-d of the main text and next section). Moreover, also as expected, we find an even lower probability of 98.3% of finding at least one self-loop for any H for $N = 10$ and $NJ_0 = 10^2$ (Fig. S4-d).

6: Relationship between gap and self-loops

In this section, we provide further evidence that self-loops can also occur outside of gaps. We restrict to $H = 0$, and we measure the probability of finding a gap P_g^0, and of the emergence of at least one self-loop starting from any

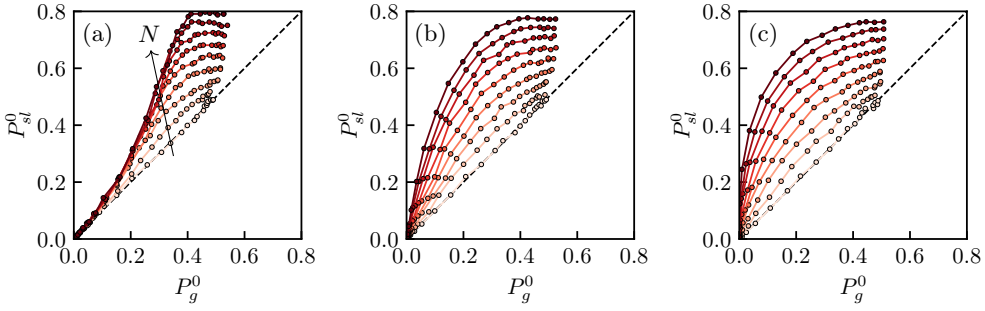

FIG. S5: **Probability of self-loops as a function of the probability of gaps** at $H = 0$, for $NJ_0 \in \left[10^{-1}, 10^2\right]$. (a) Spins ($\sigma_i = 0$). (b) Hysterons with distributed spans (σ_i flatly sampled from $[0, 0.5]$). (c) Hysterons with equal spans ($\sigma_i = 0.5$). The black dashed lines represent $y = x$; markers are color coded from light to dark red as N increases, with $N \in [2, 3, 4, 5, 6, 7, 8, 9, 10]$.

of the 2^N states P^0_{sl}, while varying J_0.

For $N = 2$ spins (Fig. S5-a), hysterons (Fig. S5-b), and hysterons with equal spans (Fig. S5-c), there is a one-to-one correspondence between the probability of gaps P^0_g and the probability of self-loops P^0_{sl}: indeed, in this case, all 4 possible states must be unstable to lead to a self-loop. However, for larger N, we systematically find more self-loops than gaps, and the difference grows with N and J_0. Interestingly, in the limit of small coupling, self-loops and gaps seem to remain equally likely for spins. In contrast, for weakly-coupled hysterons, the excess of self-loops grows with N.

7: Weak asymmetry

In this section, we reproduce the simulations of Fig. 2 of the main text, focusing on the case of hysterons with distributed spans (σ_i flatly sampled from $[0, 0.5]$), and restricted to weakly asymmetric interactions, i.e. $c_{ij}c_{ji} > 0$ for all pairs (i, j) (Figs. S6).

There are two main differences with purely random interactions. First, the probability P^0_{sl} of at least one self-loop occuring at $H = 0$ saturates toward a constant value for $NJ_0 \gg 1$ (Fig. S6-a), which *decreases* with N: the larger the system, the smaller the probability for self-loops to occur at $H = 0$. Moreover, the probability P_{sl} of finding at least one self-loops for any H saturates toward a constant value for $NJ_0 \gg 1$ (Fig. S6-b), which does not asymptote to 1 as fast as for purely random interactions, but which nevertheless increases for large N. Therefore, weakly asymmetric interactions lead to fewer self-loops than random asymmetric interactions, but we still expect that self-loops dominate the response of large, strongly coupled systems.

8: Self-loops of size $L = 4$

In this section, we focus on the emergence of $L = 4$ self-loops.

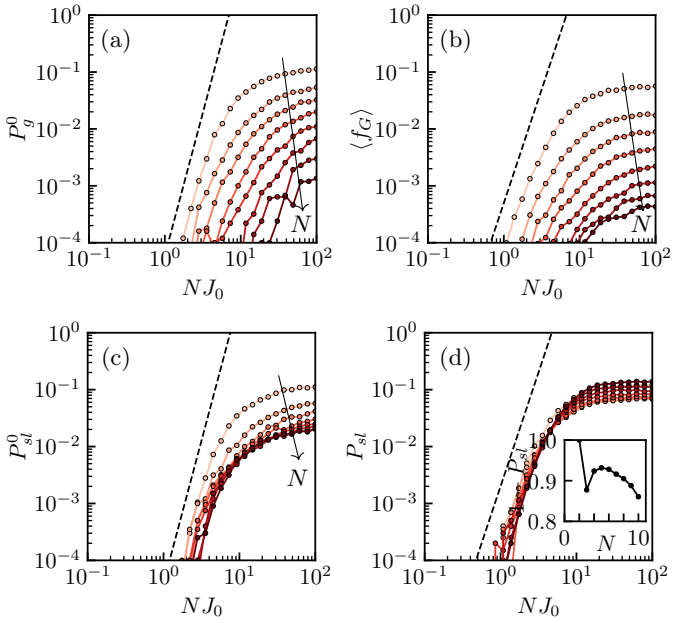

FIG. S6: **Self-loops statistics for weak asymmetric interactions between hysterons.** Statistical measures for self-loops scale when plotted as function of NJ_0 (10^5 samples; color from light to dark as N increases from 2 to 10). (a) Probability P^0_g of finding a gap at $H = 0$ (dashed line indicates slope 5). (b) Fraction of gaps f_G, defined as the mean of the ratio of the size of intervals where no stable states exist divided by $H^+(-\cdots-), H^-(+\cdots+)$ (dashed line indicates slope 4). (c) Probability P^0_{sl} of self-loops at $H = 0$ (dashed line indicates slope 5). (d) Probability P_{sl} of finding at least one self-loop for any value of H; the black dashed line represents the slope 4. Inset: The probability to be self-loop free, $1 - P_{sl}$, decays monotonously with N for large enough N, and for large couplings ($NJ_0 = 10^2$).

8.1. Gap formation mechanism for $N = 2$ coupled spins

We consider two coupled spins indexed 1 and 2, such that $h_1^+ = h_1^- = h_1^c$ and $h_2^+ = h_2^- = h_2^c$ (i.e. $\sigma_1 = \sigma_2 = 0$), where we take $h_1^c < h_2^c$. Importantly, the only possible self-loops have size $L = 4$, such that the system visits all four possible states in a cycle, and thus the self-loop must occur within a gap. We can compute the upper and lower switching fields of individual spins for each state:

$$\begin{aligned} H_1^+(--) &= h_1^c + c_{12}, \\ H_2^+(--) &= h_2^c + c_{21}, \end{aligned} \tag{S1}$$

$$\begin{aligned} H_1^-(+-) &= h_1^c + c_{12}, \\ H_2^+(+-) &= h_2^c - c_{21}, \end{aligned} \tag{S2}$$

$$\begin{aligned} H_1^+(-+) &= h_1^c - c_{12}, \\ H_2^-(-+) &= h_2^c + c_{21}, \end{aligned} \tag{S3}$$

$$\begin{aligned} H_1^-(++) &= h_1^c - c_{12}, \\ H_2^-(++) &= h_2^c - c_{21}, \end{aligned} \tag{S4}$$

and, in the limit of small couplings ($|c_{12}|$,$|c_{21}| \ll \Delta h^c$, with $\Delta h^c = h_2^c - h_1^c > 0$), the upper and lower switching fields of each state are:

$$H^+(--) = H_1^+(--) = h_1^c + c_{12}, \tag{S5}$$

$$\begin{aligned} H^-(+-) &= H_1^-(+-) = h_1^c + c_{12}, \\ H^+(+-) &= H_2^+(+-) = h_2^c - c_{21}, \end{aligned} \tag{S6}$$

$$\begin{aligned} H^-(-+) &= H_2^-(-+) = h_2^c + c_{21}, \\ H^+(-+) &= H_1^+(-+) = h_1^c - c_{12}, \end{aligned} \tag{S7}$$

$$H^-(++) = H_2^-(++) = h_2^c - c_{21}. \tag{S8}$$

Note that $H^+(--) = H^-(+-)$ and $H^+(+-) = H^-(++)$: the upper switching field of the state "below" coincides with the lower switching field of the state "above" (Fig. S7-a). Therefore, in the limit of small couplings, the convention $h_1^c < h_2^c$ enforces the structure of the Preisach graph represented in Fig. S7-a. Moreover, as the zero-coupling ordering of the states $(--) \leftrightarrow (+-) \leftrightarrow (++)$ is preserved, no gap can open, even with finite interactions.

One hole may open in two mutually-excluding cases: when the ordering of the switching fields in state $(--)$ (resp. $(++)$) is reversed. We focus on the first case without loss of generality. The condition $H_2^+(--) < H_1^+(--)$ translates into:

$$\Delta c > \Delta h^c, \tag{S9}$$

where $\Delta c = c_{12} - c_{21}$. Let us assume the condition given by Eq. (S9) is satisfied, and analyze the other states' switching fields. First, the condition to keep the same switching fields ordering in state $(++)$ can be written as:

$$H_2^-(++) > H_1^-(++) \Leftrightarrow \Delta c > -\Delta h^c, \tag{S10}$$

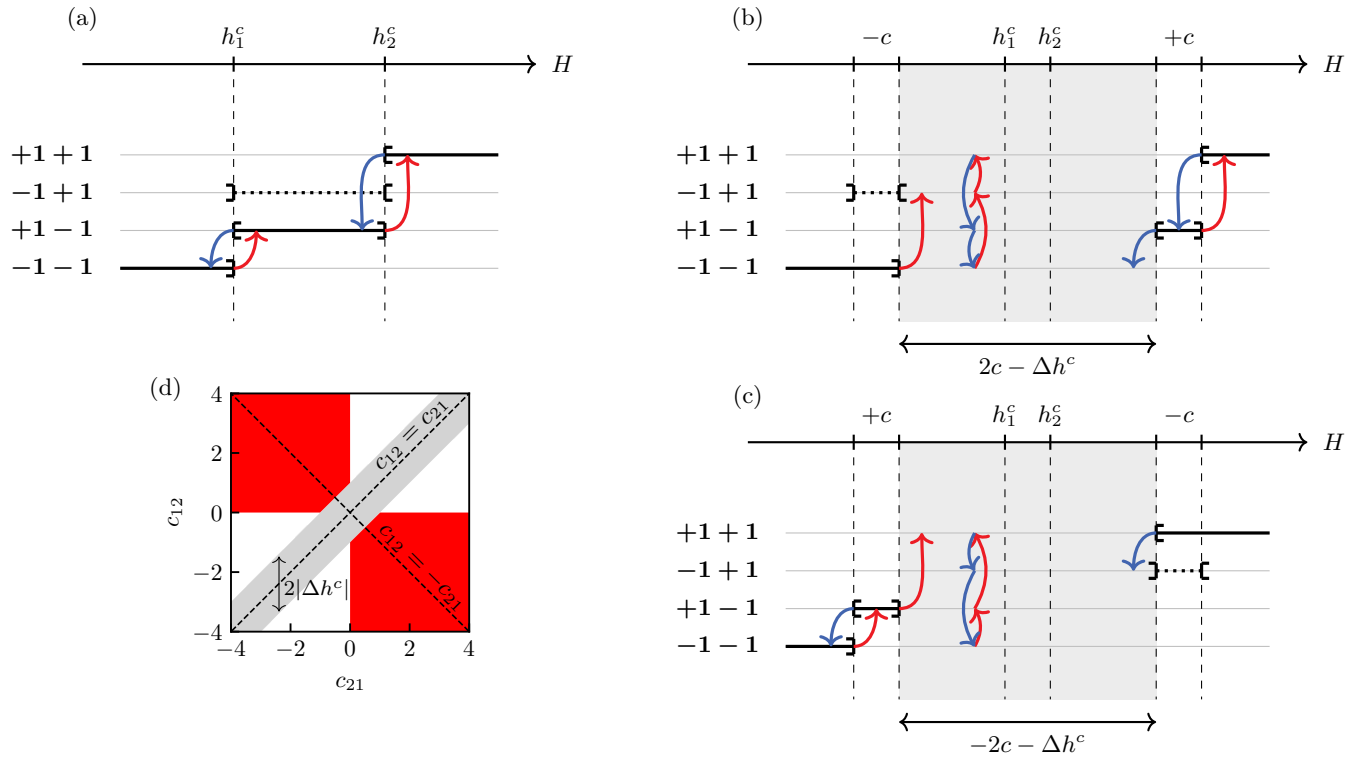

FIG. S7: **Stability ranges for $N = 2$ binary spins.** (a) Zero coupling ($c_{12} = c_{21} = 0$). (b-c) Completely asymmetric couplings $c_{12} = -c_{21} = c > 0$, i.e. $\Delta c > 0$ (b); $c_{12} = -c_{21} = c < 0$, i.e. $\Delta c < 0$ (c). The solid black, dotted black, and solid gray lines represent stable configuration, unstable configuration with 2 unstable spins, and with 1 unstable spin, respectively. Red (resp. blue) arrows represent up (resp. down) transitions. The gray area in (b-c) indicates the range of H with a gap, and the colored transitions represent the self-loop occuring within this range. (d) Portions of the (c_{12}, c_{21})-plane leading to $L = 4$ self-loops (red areas).

which is necessarily true when Eq. (S9) is satisfied. Then, the condition to open up a range of H in between the saturating states' stability ranges can be written as:

$$H_2^-(++) > H_2^+(--) \Leftrightarrow c_{21} < 0, \tag{S11}$$

imposing the sign of c_{21}. Finally, we consider the states $(+-)$ and $(-+)$. Let us start with the first one. Given $H^+(+-) = H^-(++)$, the opening of a gap inside $[H^+(--), H^-(++)]$ requires $H^-(+-) > H^+(--)$. This condition translates into:

$$H_2^+(--) < H_1^-(+-) \Leftrightarrow \Delta c > \Delta h^c, \tag{S12}$$

which is equivalent to Eq. (S9) characterizing the reversal of the critical hysteron in state $(--)$. The last condition to open a gap is that there is a finite range of H in between $H^+(-+)$ and $H^-(+-)$:

$$H^-(+-) > H^+(-+) \Leftrightarrow c_{12} > 0, \tag{S13}$$

imposing the sign of c_{12}. Altogether, the necessary and sufficient conditions for the emergence of a self-loop of size $L = 4$ in a system of $N = 2$ coupled spins can be written as:

$$\begin{aligned} \Delta c &> \Delta h^c, \\ c_{12}c_{21} &< 0. \end{aligned} \tag{S14}$$

These two conditions lead to the self-loop of size $L = 4$ represented in Fig. S7-b. The second scenario mentioned above leads to the following conditions:

$$\begin{aligned} \Delta c &< -\Delta h^c, \\ c_{12}c_{21} &< 0, \end{aligned} \tag{S15}$$

which lead to the self-loop of size $L = 4$ with the opposite "chirality", as shown in Fig. S7-c. In conclusion, couplings of opposite signs (strong asymmetry) and large enough asymmetry $|\Delta c| = |c_{12} - c_{21}|$ lead to a gap in between the saturating states (Fig. S7-d). Inside this gap, no stable state exists, which guarantees the existence of a self-loop of size $L = 4$. This is best illustrated by representing the states' stability ranges in the case of completely asymmetric interactions, i.e. $c_{12} = -c_{21} = c$, where $\Delta c = 2c$ (Figs. S7-b and c). We find that a hole of size $|\Delta c| - |\Delta h^c|$ opens in between the saturating states as soon as $|\Delta c| > |\Delta h^c|$.

8.2. $N = 2$ coupled hysterons

The conditions above can be extended to the case of hysterons with finite microscopic hysteresis:

$$\begin{aligned} |\Delta c| &> |\Delta h^c + \sigma|, \\ c_{12}c_{21} &< 0, \\ |c_{12}| &> \sigma/2, \\ |c_{21}| &> \sigma/2, \end{aligned} \tag{S16}$$

where we have considered that the two hysterons have the same microscopic hysteresis, i.e. $\sigma_1 = \sigma_2 = \sigma$. Expectedly, for larger microscopic hysteresis $\sigma > 0$, some self-loops that would have been possible for binary spins are forbidden. More precisely, self-loops emerge for larger asymmetry, i.e. $|\Delta c| > |\Delta h^c + \sigma|$, and large enough couplings, i.e. $|c_{12}| > \sigma/2$ and $|c_{21}| > \sigma/2$. Note that, similarly as for spins, self-loops emerge only when the coupling coefficients have opposite signs, i.e. $c_{12}c_{21} < 0$ (strong asymmetry).

Sampling 10^5 different instances for different σ and fixed $\Delta h^c = 1$, we represent the parameters leading to self-loops in the (c_{12},c_{21})-plane (Figs. S8). In the limit of binary spins ($\sigma = 0$), we recover the necessary and sufficient conditions for self-loops to emerge, i.e. $c_{12}c_{21} < 0$ and $|\Delta c| > |\Delta h^c|$ (Fig. S8-a). For $\sigma > 0$, numerical results are consistent with the conditions given by Eqs. (S16) (Figs. S8-b and c). We find similar results when the two hysterons' spans are different (not shown here). Altogether, at the level of $N = 2$ interacting elements, the microscopic hysteresis tends to prevent $L = 4$ self-loops that would have been possible otherwise, but in all cases strong asymmetry is a necessary condition for self-loops to emerge.

8.3. Large systems

The sufficient and necessary conditions for $L = 4$ self-loops to emerge in systems of $N = 2$ spins can be extended into necessary conditions for arbitrary N. Starting with spins and noting that each $L=4$ self-loop only involves two spins (k and l), we find that such $L=4$ loop can only occur when $c_{kl}c_{lk} < 0$ and $|\Delta c_{kl}/\Delta \tilde{h}^c_{kl}| > 1$, where $\Delta c_{kl} = c_{kl} - c_{lk}$ and where

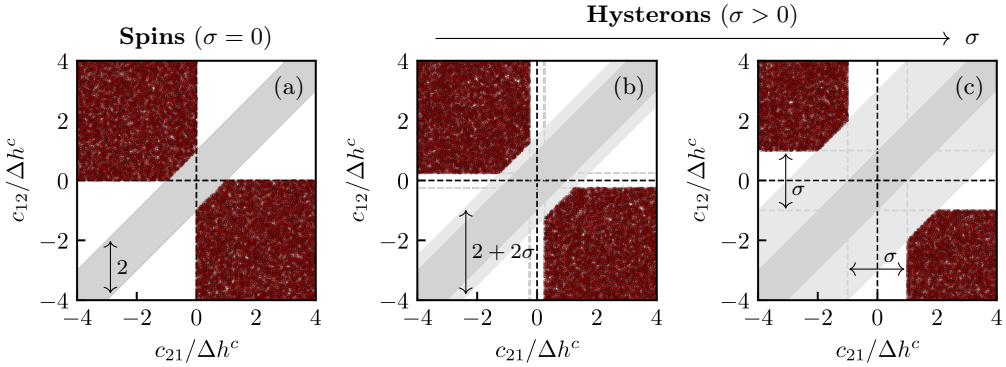

FIG. S8: **Sampling self-loops for $N = 2$ interacting elements.** Self-loops of size 4 for arbitrary interactions in the (c_{12},c_{21})-plane (red transparent markers); (a) spins, i.e. $\sigma = 0$; (b-c) hysterons, for $\sigma = 0.5$ (b) and $\sigma = 2$ (c).

$$\tilde{h}_i^c = h_i^c - \sum_{j\neq k,l} c_{ij} s_j. \tag{S17}$$

Hence, for arbitrary N, the effect of the $N-2$ spins that do not flip is to effectively rescale the difference between the switching fields of the two flipping spins. Therefore, the same as for $N=2$, self-loops of size $L=4$ only emerge for strong asymmetry ($c_{kl}c_{lk}<0$) and large enough asymmetry $|\Delta c_{kl}|$. However, in contrast with $N=2$, when a pair of spins satisfies the conditions above, it does not imply that the system necessarily reaches this cycle, as it might be disconnected from the stable states.

We confirm the results above by sampling 10^5 systems with $N=1024$ elements, and looking for self-loops at any H. We plot a red marker in the rescaled (c_{12},c_{21})-plane when we find a $L=4$ self-loop, where 1 and 2 now represent the two flipping elements. We focus on the large coupling limit ($NJ_0=10$), for collections of spins (Fig. S9-a) and hysterons (Fig. S9-b).

We first focus on the case of spins. When self-loops occur, we find they are necessary included in the region of the rescaled (c_{12},c_{21})-plane where $L=4$ self-loops occur for $N=2$ spins. However, for some systems there exist pairs of spins which are in the *red* region (for a given configuration of the rest of the system), but which are never involved in a $L=4$ self-loop. The situation is very similar for hysterons with distributed spans: we find self-loops in the same region as for spins, though there are fewer self-loops, especially close to the boundaries.

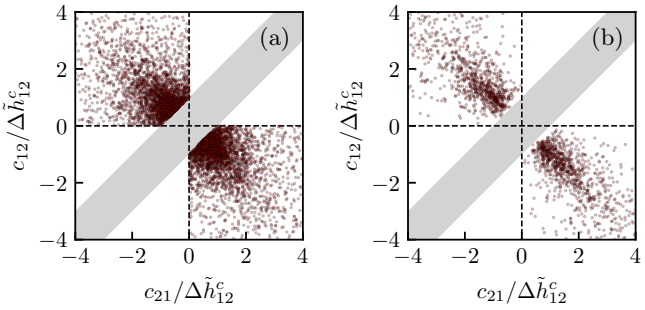

FIG. S9: **Self-loops of size 4 in large systems.** $L=4$ Self-loops for arbitrary interactions in the ($c_{12}-c_{21}$) plane (red transparent markers); in the limit of binary spins (a), i.e. $\sigma_i=0$, and for hysterons (b), i.e. with σ_i flatly sampled from $[0,0.5]$; fixed $N=1024$, and $NJ_0=10$.

8.4. Preventing $L=4$ self-loops

We note that the condition to prevent $L=4$ self-loops consists of a simple and a complex part, and we refer to the simple part - $c_{ij}c_{ji}>0$ for all pairs (i,j) - as the condition of weak asymmetry. This simple condition is sufficient to guarantee the absence of $L=4$ self-loops for any system size, although, as there are other parts in hysteron parameter space where such self-loops are prohibited - it is overly restrictive.

9: Strictly self-loop free ensembles

In this section, we discuss the different classes of strictly well-behaved ensembles.

9.1. Symmetric interactions

Symmetric interactions are reminiscent of dilute interacting soft spots, as discussed in [5]. Soft spots correspond to local rearrangements associated with quadrupolar Eshelby-like displacement fields (Fig. S10-a). In this context, the binary elements are modeled as having the same sizes, which implies $c_{ij}=c_{ji}$, and the sign of the interaction coefficient is given by their relative orientations. When compatible lobes of the fields face each other, the interaction is rather ferromagnetic ($c_{ij}>0$), while it is rather antiferromagnetic ($c_{ij}<0$) when incompatible lobes face each other.

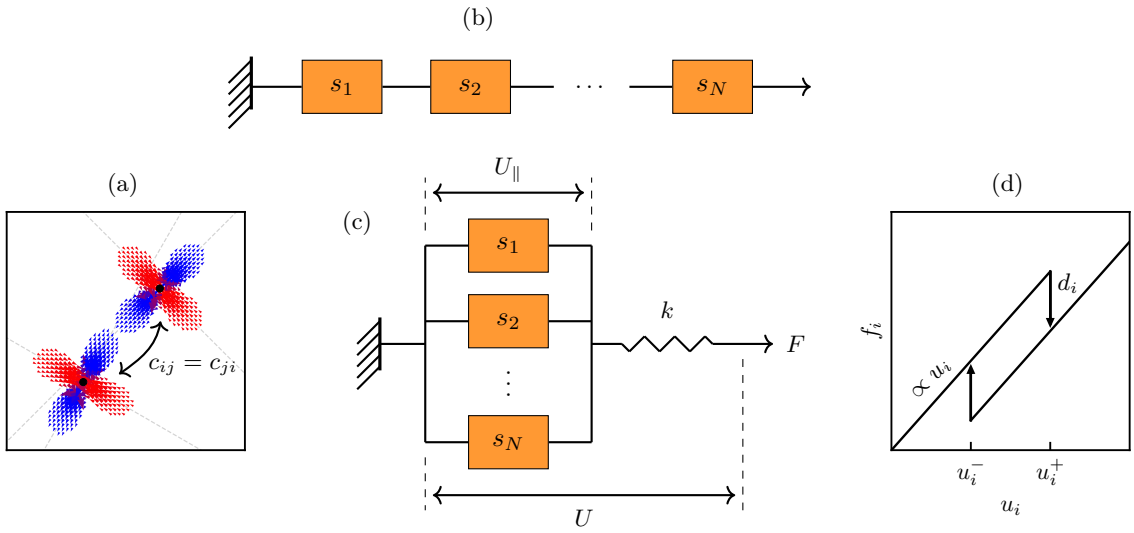

FIG. S10: **Realizations of the different interaction classes.** (a) Symmetric interactions: two interacting soft spots, associated with quadrupolar displacement fields, interact symmetrically: blue arrows: inward displacements; red arrows: outward displacements. In this example, the orientations of the quadrupoles are such that $c_{ij} = c_{ji} < 0$ due to the incompatibility of the quadrupolar fields. (b) Constant-columns interactions: linear chain of mechanical hysterons. (c) Ferromagnetic interactions: parallel arrangement of mechanical hysterons in series with a spring of stiffness k and zero-rest-length. (d) Force-displacement curve for a single mechanical hysteron.

9.2. Constant-columns interactions

Constant-columns interactions occur in a linear chain of bistable springs (Fig. S10-b), if we assume that the force-displacement curve of such a mechanical hysteron is given by a bilinear relation:

$$f_i = u_i - d_i s_i, \tag{S1}$$

with f_i the force, u_i the displacement, d_i the force discontinuity and s_i the state (Fig. S10-d). This system can be mapped on the pairwise interacting hysteron model, where $c_{ij} = -d_j$ with $d_j > 0$, where $H = U = \sum_i u_i$ is the total displacement [12].

9.3. Ferromagnetic interactions

Ferromagnetic interactions occur, for example, in a parallel arrangement of mechanical hysterons in series with a spring of stiffness k [26] (Fig. S10-d). The mapping then is $c_{ij} = d_j/k$ with $d_j > 0$, where $H = U$ is the total displacement [26]. Note that a collection of hysterons arranged in parallel as represented in Fig. S10-c interact ferromagnetically, and the interaction matrix has a constant-columns structure.

9.4. Constant-rows interactions

The case of constant-rows interactions is relatively artificial as it corresponds to a case where hysterons are affected by the flipping of any other hysteron in exactly the same way. We do not know if this interaction matrix can be derived from mechanical equilibrium of mechanical hysterons.

10: Role of the race condition rules

In this section, we analyze the impact of different race condition rules on the probability of finding self-loops and on the self-loop size distribution. We explore four different dynamical rules. Rule 0 considers the model ill-defined whenever race conditions occur [12, 21] (discarding the associated instance), and prevents sampling large systems (see section 2). Rule 1 (focus of the main text) and 1′ specify to flip only the most and the least unstable element,

respectively. Finally, under rule 2, all unstable elements are flipped simultaneously. Table SI summarizes the ill-defined conditions encountered in each interaction ensemble for the different race condition rules.

Interaction ensemble	**rule 0**	**rule 1**	**rule 1′**	**rule 2**
Arbitrary	RC/G/SL	G/SL	G/SL	G/SL†
Symmetric	RC	–	–	SL*
Constant-columns	RC	–	–	SL*
Constant-rows	RC	–	–	SL*
Ferromagnetic	RC	–	–	–

* $L = 2$ self-loops only. † All $L \geq 2$ self-loops allowed.

Table SI: Summary of the occurrence of ill-defined conditions for various interaction ensembles and race condition rules: RC: race conditions; G: gaps; SL: self-loops.

10.1. Arbitrarily-coupled hysterons

Here, we examine different race condition rules for hysterons with random asymmetric interactions. First, in the case where all unstable hysterons flip simultaneously (rule 2), we find that all self-loop sizes are allowed starting from $L = 2$ (Fig. S11-h). In contrast, all race conditions rules which involve flipping elements one by one (rules 0, 1, and 1′) lead to self-loops whose sizes are always even, starting from $L = 4$ (Figs. S11-e to g). This parity is expected given all the hysterons involved in a self-loop must first flip and then unflip to revisit a state.

Let us first show that self-loops of size $L = 2$ are forbidden when hysterons flip one-by-one, because they correspond to loops involving a single hysterons with negative span. Let us consider that state S is unstable at a given value of the drive H because hysteron i is unstable, e.g. $H > H_i^+(S)$ (without loss of generality). The system enters a

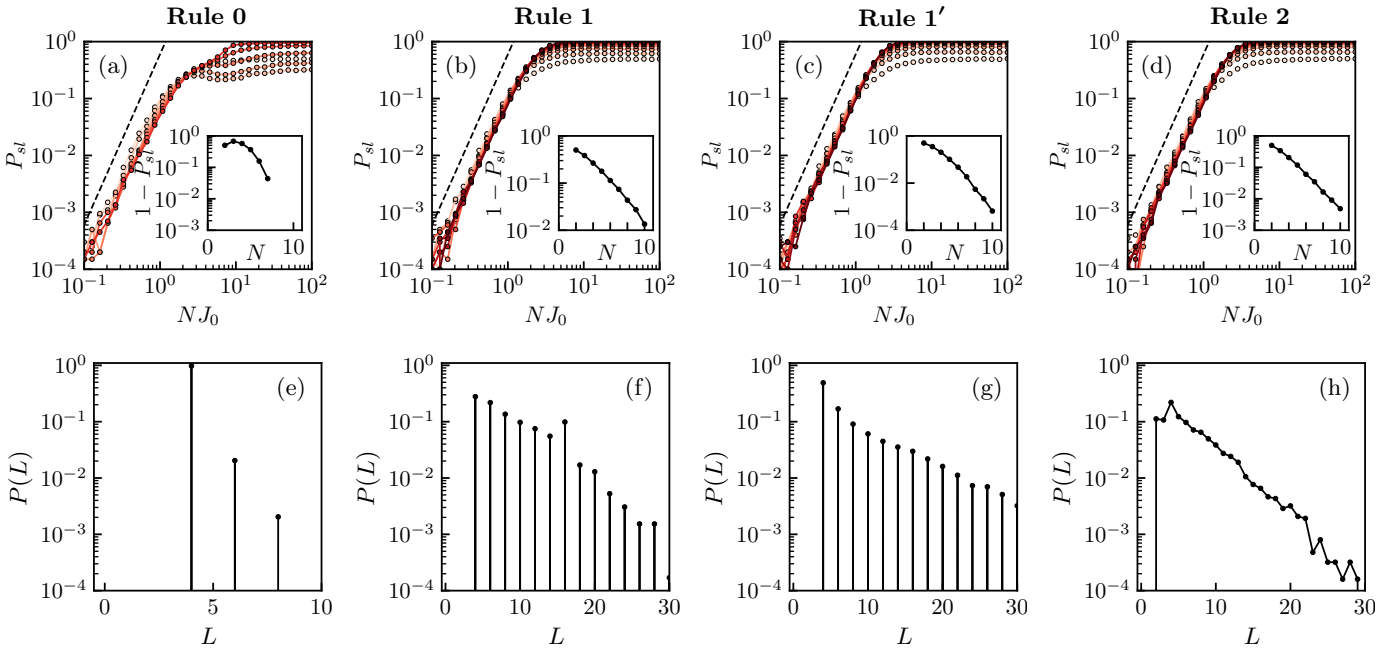

FIG. S11: **Self-loop statistics for arbitrarily-coupled hysterons and different race condition rules.** (a-d) Probability P_{sl} of at least one self-loops occurring for any H as a function of NJ_0, for different $N \in [2, 3, \ldots, 10]$, color-coded from light to dark red as N increases; the black dashed lines represent the slope 3; (inset) probability to be self-loop free $1 - P_{sl}$ as a function of N in the large coupling limit ($NJ_0 = 10^2$). (e-h) Self-loops size distributions for fixed $NJ_0 = 20$ and $N = 8$. (a/e) Rule 0; (b/f) rule 1; (c/g) rule 1′; (d/h) rule 2.

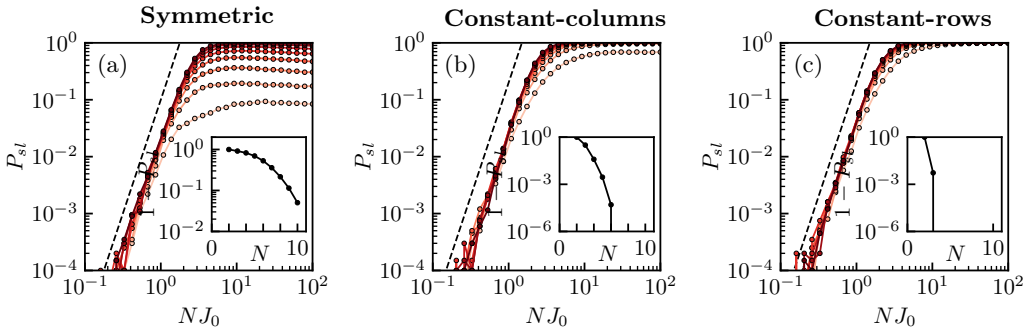

FIG. S12: **Self-loop statistics for well-behaved models of coupled hysterons**, where race conditions are resolved with rule 2. Statistical measures for self-loops scale when plotted as function of NJ_0 and dominate for $NJ_0 \gg 1$ (10^5 samples; color from light to dark as N increases from 2 to 10). Probability P_{sl} of finding at least one self-loop for any value of H (dashed line indicates slope 4). Inset: The probability to be self-loop free, $1 - P_{sl}$, decays to zero with N for large couplings ($NJ_0 = 10^2$). (a) Symmetric interactions; (b) constant-columns interactions; (c) constant-rows interactions.

self-loop of size 2 if hysteron i remains unstable after the snap, i.e. $H < H_i^-(S)$, which yields:

$$h_i^- - \sum_{j\neq i} c_{ij}s_j > h_i^+ - \sum_{j\neq i} c_{ij}s_j. \tag{S1}$$

All hysterons $j \neq i$ being unchanged, Eq. (S1) implies $h_i^- > h_i^+$, which corresponds to hysteron i having a negative span, i.e. $\sigma_i < 0$, which is forbidden (excluded from our sampling).

Interestingly, for all race condition rules, the probability P_{sl} of finding at least one self-loop increases as a power law for $NJ_0 \ll 1$, and saturates toward a constant value with J_0 for $NJ_0 \gg 1$ (Figs. S11-a to d). Similar dependencies have been observed for other properties of interacting hysterons [4, 21, 30]. Except for rule 0, the large-J_0 plateau value increases monotonically with N, and in all cases the data suggest that $P_{sl} \to 1$ when N increases. Moreover, in all cases, the size of self-loops seems to be exponentially distributed, modulo the specific constraints on the self-loop sizes discussed above.

10.2. Well-behaved ensembles

Here, we focus on the well-behaved models introduced in the main text, namely symmetric, constant-columns, constant-rows, and ferromagnetic interactions. We have shown that self-loops are forbidden for all these classes when hysterons flip one by one (rules 0, 1 and 1′). Here, we analyze the probability of finding self-loops and the self-loop size distributions when race conditions are resolved with rule 2.

Let us first focus on symmetric, constant-columns, and constant-rows interactions. We find that all self-loops have size $L = 2$, independently of the model (not shown here). The presence of 2-cycles is a well-known feature for symmetrically-coupled spins where all unstable spins flip simultaneously [33, 34, 37], which is generally called synchronous or parallel update in the context of spin glasses and neural networks. Second, the probability P_{sl} of finding at least one $L = 2$ self-loop for any H increases as a power law for $NJ_0 \ll 1$, and saturates toward a constant value with J_0 for $NJ_0 \gg 1$ (Figs. S12), which asymptotes to 1 as N increases (Figs. S12-insets)

Finally, for purely ferromagnetic interactions, we find no self-loops when race conditions are resolved with rule 2, which suggests that the 2-cycles emerging with rule 2 are more related to the presence of antiferromagnetic interactions than to non-symmetric ones, which is very different than in the case where hysterons flip one by one.

11: The combinatorics and structure of self-loops

We examine the proliferation of self-loops using a suite of combinatorial and numerical tools we recently developed for studying transition graphs in hysteron models [31]. Transition graphs have emerged as a powerful framework for capturing and studying sequential responses [3, 18, 21, 31]. In these, states S are represented by nodes, and their transitions under zero-temperature, quasistatic driving with a global field H, form directed edges (Fig. 1-c of the main text, and Figs. S16). The range of stability of state S is given by its upper and lower switching fields $H^{\pm}(S)$ (which follow from the extrema of $H_i^{\pm}(S)$, see main text), and an up or down transition is initiated when $H > H^+(S)$ or $H < H^-(S)$. Here, we use this framework to represent the structure of self-loops, focusing on the repeating cycle of their unstable states.

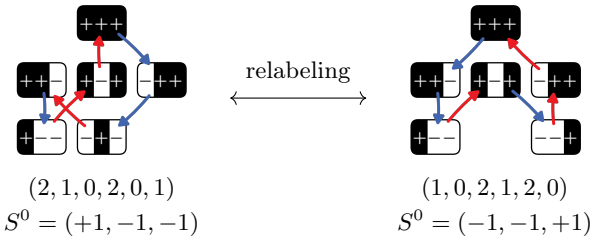

FIG. S13: **Relabeling symmetry.** Each self-loop is defined by the sequence of flips and the starting state S^0. Two self-loops are equivalent if one can be obtained from the other by a relabeling of the hysterons.

11.1. Structure of self-loops

Here we discuss how to count the number of fundamental self-loop structures of size L and involving n_e elements, $M(n_e, L)$, irrespective of whether they are realizable in a certain interaction ensemble. We first determine all potential self-loops using a naive procedure based on the combinatorics of flip sequences, which generates cycles of length L on a (n_e)-hypercube. However, many of these are related under two trivial symmetries—relabeling and timeshifting (see below)—and in the second step we determine the fundamental self-loops, i.e., those that can not be mapped onto each other by trivial symmetries.

To illustrate this, consider $M(3, 6)$. A naive count works as follows: there are 24 self-loops of length $L = 6$ starting from, e.g., state $S = (-1\,-1\,-1)$, yielding a total of $2^3 \times 24 = 192$ potential self-loops. To find the fundamental self-loops, we discuss two symmetries on their structure, i.e., sequence of states. First, we consider self-loops equivalent if they can be mapped onto each other by relabeling of the hysterons, which reduces the number of loops by a factor $n_e!$ (Fig. S13). Note, however, that each of these corresponds to a separate polytopes in parameter space. Second, since any state in a self-loop can be taken as the starting state, we consider self-loops equivalent if they can be mapped on each other by a 'timeshift' (Fig. S14-S15). We note that all loops related by shifts lead to the same polytope in parameter space. For the example of $n_e = 3, L = 6$, the relabeling symmetry reduces the 192 potential self-loops to 32, and the timeshift symmetry lowers it further to six distinct fundamental self-loops (Fig. S16).

We now describe our algorithm for calculating $M(n_e, L)$. We specify each self-loop by its starting state S^0 and the sequence of element flips (Fig. S13). The relabeling symmetry implies that the sequence of flips $(2, 1, 0, 2, 0, 1)$ from state $S^0 = (+1\,-1\,-1)$ gives rise to the same self-loop as the sequence $(1, 0, 2, 1, 2, 0)$ from state $S^0 = (-1\,-1\,+1)$. We break this permutation symmetry by indexing hysterons according to the order in which they are flipped, and only keeping loops where the different hysteron flips occur in descending order, such as $(2, 1, 0, \dots)$ and $(2, 1, 2, 0, \dots)$. Using this convention, we only keep the first sequence $(2, 1, 0, 2, 0, 1)$, and overall this convention reduces the number of generated self-loops by a factor $n_e!$.

Second, we deal with the timeshift symmetry. For example, the sequence $(2, 1, 0, 2, 0, 1)$ from state $(+1\,-1\,-1)$ can also be 'shifted' by one, such that we obtain the sequence $(1, 0, 2, 0, 1, 2)$ starting from state $(+1\,-1\,+1)$; with the relabeling convention described above, these cycle maps to $(2, 1, 0, 1, 2, 0)$ starting from state $(+1\,+1\,-1)$ (Fig. S14). For computational efficiency, we break up the check for timeshift symmetry in two parts.

First, when generating self-loops, we order these by their minimum magnetization $m := \sum_i s_i$:

$$M(n_e, L) = \sum_{m=-n_e}^{n_e} M_m(n_e, L) \tag{S1}$$

where $M_m(n_e, L)$ is the number of self-loops which starts and ends at the same magnetisation m, and does not go

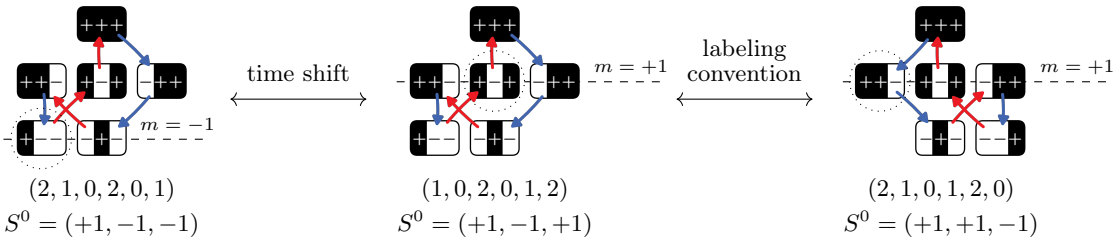

FIG. S14: **Time shift symmetry between two self-loops.** Each self-loop is defined by the sequence of flips and the starting state S^0. Two self-loops are the same if one can be obtained from the other by arbitrarily shifting the starting state. This ambiguity on the starting state is partially lifted by decomposing self-loops by the magnetization m of their starting state, and imposing the magnetization cannot go below m.

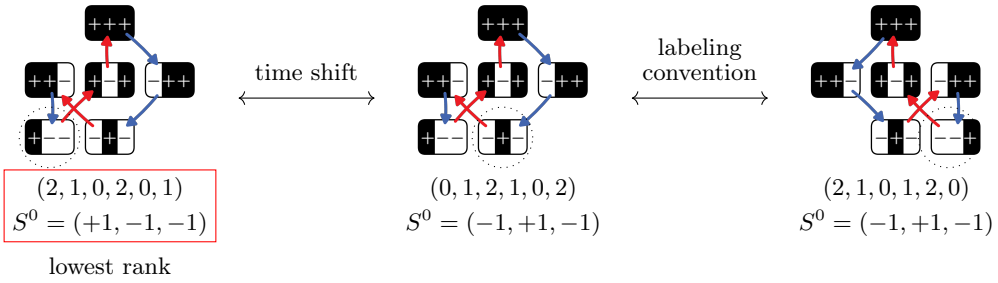

FIG. S15: **Time shift symmetry between two self-loops.** To remove the final ambiguity on the starting state when there exist multiple possible starting states with the same magnetization, we compare the ranking of self-loops (see text), and pick the loop with the smallest ranking.

below m. Hence, we first generate all loops starting at state $(-1, -1, -1, \dots)$ with magnetization $m = -n_e$; then we start at states with magnetization $m = -n_e + 2$, but whenever such potential loop reaches a lower magnetization, we dismiss it. This approach filters out loops such as $(2, 1, 0, 1, 2, 0)$ starting from state $(+1 + 1 - 1)$. Iterating over all magnetizations is computationally effective, e.g., for $n_e = 3, L = 6$, this procedure reduces the number of potential self-loops from 32 to 7.

The labeling and magnetization conventions limit the number of self-loop structures, but do not fully eliminate all duplicates. For our example, both loops $(2, 1, 0, 2, 0, 1)$ from state $(+1 - 1 - 1)$ and $(2, 1, 0, 1, 2, 0)$ from state $(-1 + 1 - 1)$ would be included, even though there are related by shifting and relabeling (Fig. S15). To select which of these to keep, we assign to each of these loops a ranking composed of the initial state and the sequence of flipped hysterons: in the above example these rankings would be 100210102 and 010210120 (where we replaced all the phases -1 by 0 for notational convenience). For equivalent loops, we only include the loop with the lowest ranking. This allows us to identify one more pair of duplicates for $n_e = 3, L = 6$ – namely, the two loops described above – bringing the final number of $(n_e = 3, L = 6)$ fundamental self-loops down to 6, as shown in the main text.

We implement this procedure using a suite of numerical tools developed earlier [31], and summarize the results in Table SII and Fig. S16. Our results show a rapid proliferation of the number of fundamental self-loops when L and n_e increase.

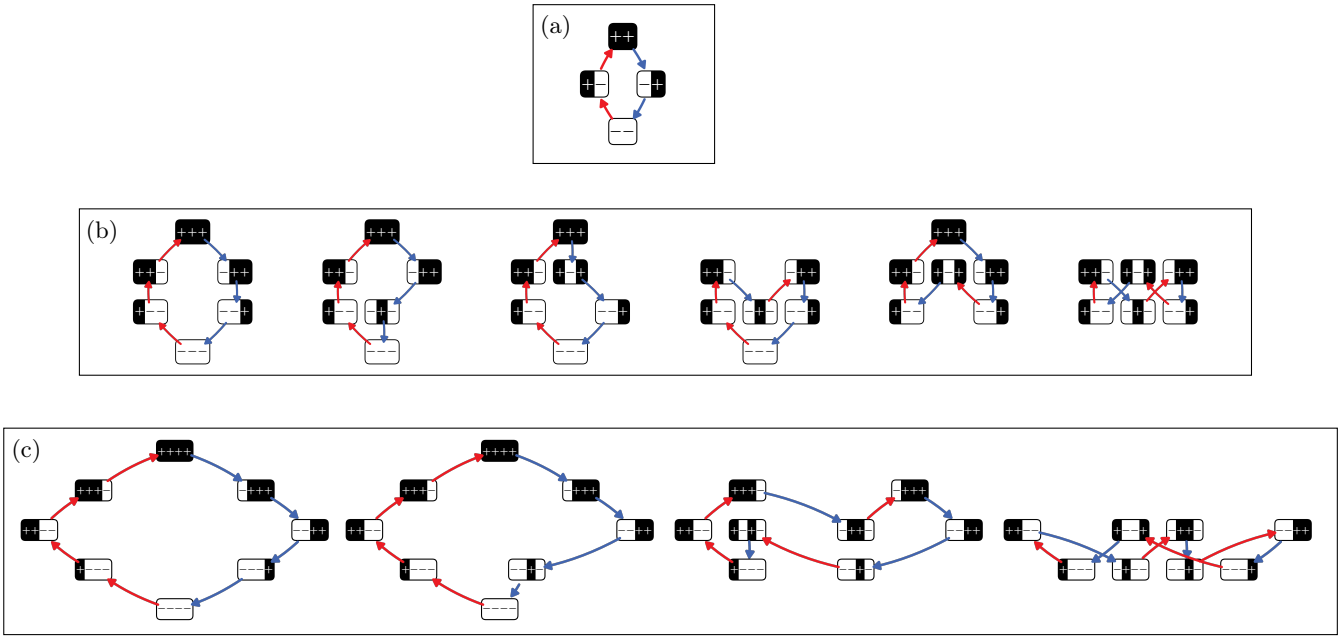

FIG. S16: **Ensembles of fundamental self-loops of different sizes.** Blue(/red) arrows represent up(/down) transitions. (a) Size $L = 4$ (1 self-loop). (b) Size $L = 6$ (6 self-loops). (c) Size $L = 8$ (58 self-loops, not all shown).

	$n_e = 2$	$n_e = 3$	$n_e = 4$	$n_e = 5$
$L = 4$	1	–	–	–
$L = 6$	–	6	–	–
$L = 8$	–	2	56	–
$L = 10$	–	–	176	796
$L = 12$	–	–	420	9028
$L = 14$	–	–	448	76640
$L = 16$	–	–	112	535584
$L = 18$	–	–	–	x
$L = 20$	–	–	–	x
$L = 22$	–	–	–	x
$L = 24$	–	–	–	x
$L = 26$	–	–	–	x
$L = 28$	–	–	–	x
$L = 30$	–	–	–	x
$L = 32$	–	–	–	15109096

Table SII: **Number fundamental self-loop structures which can be drawn**. The left column (resp. top row) indicates the size L of self-loops (resp. the number of hysterons involved in the loop n_e); the number inside each box is the number of different self-loop structures that can be drawn (not all of them are realizable with pairwise interactions).

	$n_e = 2$	$n_e = 3$	$n_e = 4$	$n_e = 5$
$L = 4$	1	–	–	–
$L = 6$	–	6	–	–
$L = 8$	–	0	56	–
$L = 10$	–	–	114	796
$L = 12$	–	–	145	x
$L = 14$	–	–	48	x
$L = 16$	–	–	4	x
$L = 18$	–	–	–	x
$L = 20$	–	–	–	x
$L = 22$	–	–	–	x
$L = 24$	–	–	–	x
$L = 26$	–	–	–	x
$L = 28$	–	–	–	x
$L = 30$	–	–	–	x
$L = 32$	–	–	–	x

	$n_e = 2$	$n_e = 3$	$n_e = 4$	$n_e = 5$
$L = 4$	0	–	–	–
$L = 6$	–	2	–	–
$L = 8$	–	0	24	–
$L = 10$	–	–	4	376
$L = 12$	–	–	1	x
$L = 14$	–	–	0	x
$L = 16$	–	–	0	x
$L = 18$	–	–	–	x
$L = 20$	–	–	–	x
$L = 22$	–	–	–	x
$L = 24$	–	–	–	x
$L = 26$	–	–	–	x
$L = 28$	–	–	–	x
$L = 30$	–	–	–	x
$L = 32$	–	–	–	x

Table SIII: **Number of fundamental self-loop structures which are realizable**. The left column (resp. top row) indicates the size L of self-loops (resp. the number of hysterons involved in the loop n_e); the number inside each box is the number of different self-loop structures which are realizable (left), and which are realizable when restricting to weak asymmetry (right).

11.2. Realizability of self-loops

Now that we have established the structure of the fundamental self-loops as a function of (n_e, L), we determine their realizability. For every fundamental self-loop we can construct a set of linear inequalities of the hysteron parameters $(h_i^{\pm}, c_{ij})$ using linear programming [21, 30]. We adapt the methods introduced in [31] to deal with self-loops and race conditions, and eliminate the role of the value of the driving parameter.

The framework in [31] did not explicitly discuss parameter conditions to realize self-loops, but instead focused on non-loop transitions, for which separate design inequalities for the initial, intermediate and final state of an avalanche were derived. As self-loops have no final state, it suffices to construct the initial and intermediate inequalities. Moreover, we are not interested in whether a self-loop arises for a specific value of the driving H, but only whether a self-loop is realizable for *any* driving. We account for this by eliminating the driving from the set of linear inequalities. For example, if we have the set of design inequalities:

$$\begin{aligned} &H > H^+(S^0),\\ &H < H^-(S^1),\\ &H > H^+(S^2),\\ &H < H^-(S^3),\\ &H > H^+(S^4),\\ &H < H^-(S^5), \end{aligned} \tag{S2}$$

which realizes a self-loop of length $L = 6$ and driving H, we can eliminate the driving H to obtain inequalities that enforce that there is a range of the driving H where a self-loop occurs:

$$\begin{aligned} &H^-(S^1) > H^+(S^0),\\ &H^-(S^1) > H^+(S^2),\\ &H^-(S^1) > H^+(S^4),\\ &H^-(S^3) > H^+(S^0),\\ &H^-(S^3) > H^+(S^2),\\ &H^-(S^3) > H^+(S^4),\\ &H^-(S^5) > H^+(S^0),\\ &H^-(S^5) > H^+(S^2),\\ &H^-(S^5) > H^+(S^4). \end{aligned} \tag{S3}$$

While previously, we considered transitions with race conditions ill-defined in [31], we can easily implement our resolution of the race conditions by flipping the most unstable hysteron. We note that as a consequence we do not need to keep track of all switching fields $H_i^{\pm}(S)$, but only of the state switching fields $H^{\pm}(S)$.

We finally note subtlety for states that are 'unconditionally unstable' – i.e., for which $H^-(S) > H^+(S)$. While these states pose no issue if $H < H^+(S)$ or $H > H^-(S)$, the range $H^+(S) < H < H^-(S)$ is problematic, as in this case one cannot judge whether a hysteron flips up or down from the ordering of the switching fields alone. As a proper accounting for these cases would significantly increase the complexity of the inequalities, we choose to take a more conservative approach, where a self-loop is counted as non-realizable if it is contingent upon this exceptional case.

The results of our realizability checks for the general case and weakly asymmetric case are shown in Tables SIII.

12: Response for strictly self-loop-free ensembles

The absence of self-loops in the different well-behaved models allows to explore statistics of avalanches and of the response to cyclic drive for large N and arbitrary J_0. We focus below on race condition rule 1, where the most unstable element flips first, and on ensembles of hysterons with distributed spans (σ_i flatly sampled from $[0, 0.5]$).

12.1. Avalanche sizes

We consider $N = 1024$ hysterons and place ourselves at $H = 0$. Starting from a random initial state, the system is stabilized by flipping unstable hysterons one by one until a stable state S^0 is found (which is guaranteed in the absence of self-loops). We simulate $S^0 \to S^1$ over 5×10^3 samples, and record the avalanche sizes A – the number of flips before the system settles in a stable state. For all ensembles, when $NJ_0 \ll 1$, only Preisach-like non-avalanche transitions ($A = 1$) are found. For symmetric interactions, the larger J_0, the broader the avalanche size distribution and the larger the mean avalanche size, with a crossover around $NJ_0 \simeq 1$ (Figs. S17-a and d). For $NJ_0 \gg 1$, avalanche sizes are power-law distributed with a cutoff growing with J_0 and N, and saturating below system size. For constant-columns interactions, we find a similar transition scenario at $NJ_0 \simeq 1$ (Figs. S17-b and e). However, for $J_0 \simeq 1$, the mean avalanche size reaches a maximum, which increases with system size (Fig. S17-e, inset), and then decreases abruptly, and increases again for larger J_0. Finally, for constant-rows interactions, numerical simulations confirm that transitions can only be Preisach-like nonavalanche transitions or avalanches of size 2 that do not alter the magnetization $m = \sum_i s_i$ (Figs. S17-c and f), with a crossover between the two around $NJ_0 \simeq 1$.

12.2. Response to cyclic drive

Let us now consider cyclic drive conditions - when the input U is swept between $U_{\min}$ and $U_{\max}$. We focus on two aspects of the response: the number of driving cycles τ taken to reach a periodic orbit, and the period T of the orbit relative to the driving cycle. In the Preisach model (limit of zero interactions), $\tau \leq 1$ and $T = 1$, which can be understood by noting that each (independent) hysteron requires at most one cycle before it reaches a periodic orbit. Only a few results exist for finite interactions between hysterons. For small systems, it was shown that the transients τ and periodicity T are distributed exponentially [4].

Here, we consider $N = 512$ hysterons and place ourselves at $U = 0$. Starting from a random initial condition, the system is stabilized by flipping unstable hysterons one by one until a stable state is found. Finally, the drive U is swept between 0 and $U_{\max}$, where $U_{\max}$ is the drive amplitude leading to a magnetization $m = \sum_i s_i$ equal or larger than $N/2$ ($U_{\max}$ is determined during the first drive cycle and is kept fixed for the rest of the simulation). For the symmetrically-coupled case (Figs. S18-a and d), when $NJ_0 \ll 1$, both $\langle\tau\rangle$ and $\langle T\rangle$ are equal to 1, and when $NJ_0 \gg 1$, both $\langle\tau\rangle$ and $\langle T\rangle$ are greater than 1 and constant with J_0. Remarkably, both $\langle\tau\rangle$ and $\langle T\rangle$ reach a maximum for intermediate $J_0 \simeq 1/N$ [21]. For constant-columns and constant-rows interactions, we systematically find $T = 1$ (Figs. S18-b and c): all orbits have the same period as the drive. This is expected for constant-columns

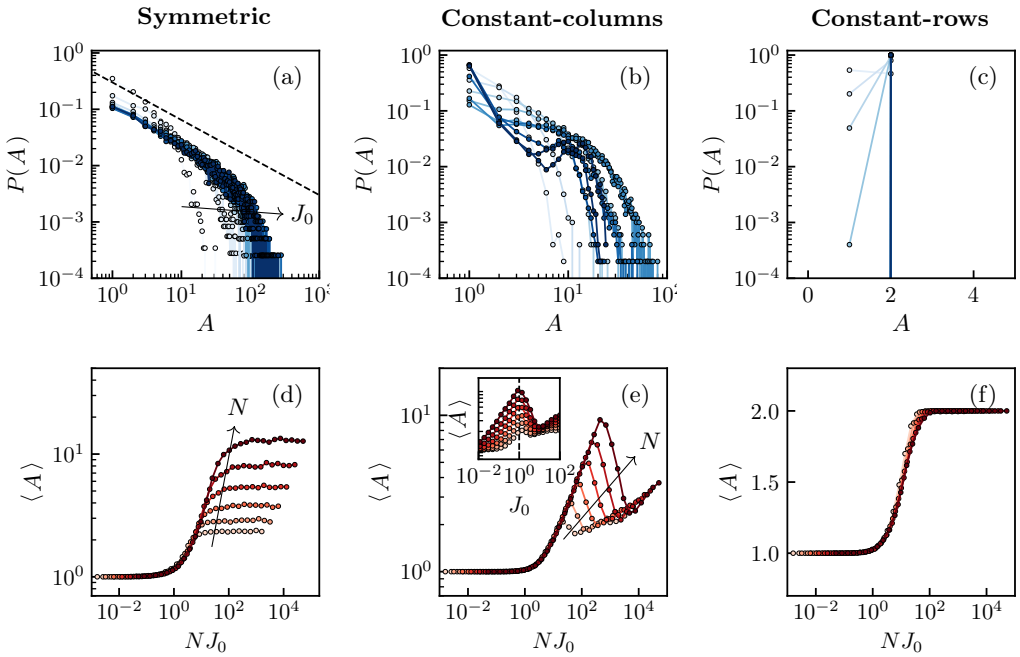

FIG. S17: **Large avalanches for well-behaved models**. (a-c) Avalanche size distributions for different $J_0 \in [10^{-2}, 10^2]$; color-coded from light to dark blue as J_0 increases; fixed $N = 1024$. (d-f) Mean avalanche size $\langle A\rangle$ as a function of NJ_0, for different $N \in [16, 32, 64, 128, 256, 512]$, color-coded from light to dark red as N increases. (a/d) Symmetric interactions; (b/e) constant-columns interactions; (c/f) constant-rows interactions.

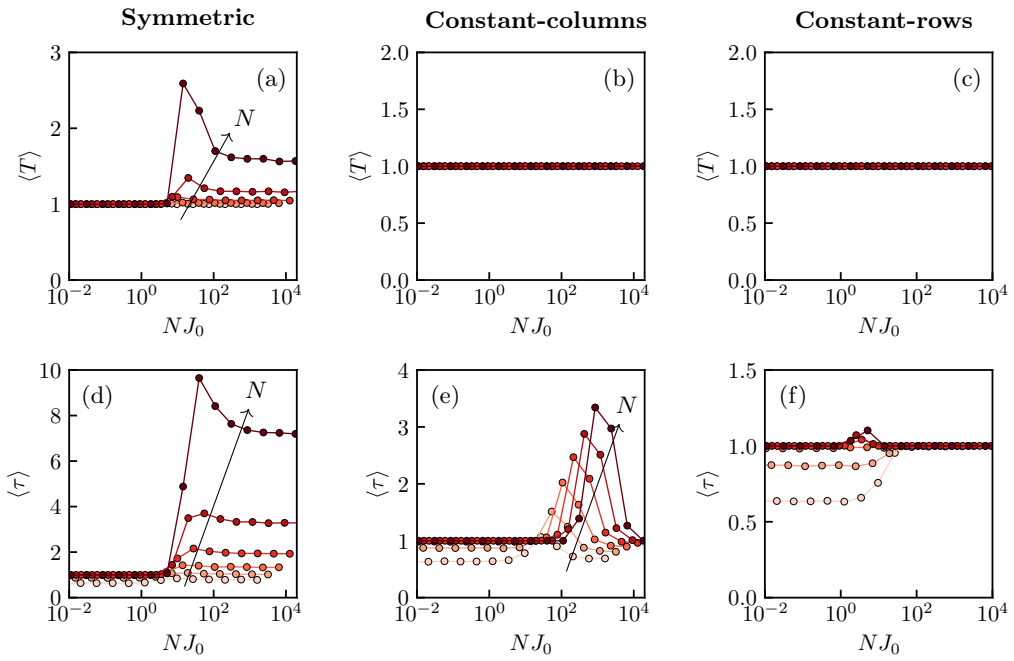

FIG. S18: **Transients and periodicity during cyclic drive for the well-behaved models**, for different $N \in [16, 32, 64, 128, 256, 512]$, color coded from light to dark red as N increases. (a-c) Ensemble averaged transient length $\langle\tau\rangle$ as a function of J_0. (d-f) Ensemble averaged periodicity $\langle T\rangle$ as a function of J_0. (a/d) Symmetric interactions; (b/e) constant-columns interactions; (c-f) constant-rows interactions.

interactions given the absence of scrambling [12]. Also, $\langle\tau\rangle = 1$ for both $NJ_0 \ll 1$ and $NJ_0 \gg 1$ (Figs. S18-e and f). For constant-columns interactions, $\langle\tau\rangle$ reaches a maximum for intermediate J_0 at the same value corresponding to the maximum of $\langle A\rangle$, i.e. $J_0 \simeq 1$. In contrast, for constant-rows interactions, the maximum of $\langle\tau\rangle$ is reached for $J_0 \simeq 1/N$.